HHS Public Access

Author manuscript

Cell Rep. Author manuscript; available in PMC 2021 September 10.

Published in final edited form as:

Cell Rep. 2021 August 24; 36(8): 109586. doi:10.1016/j.celrep.2021.109586.

Hemozoin-mediated inflammasome activation limits long-lived anti-malarial immunity

Angela D. Pack[1], **Patrick V. Schwartzhoff**[1], **Zeb R. Zacharias**[2], **Daniel Fernandez-Ruiz**[3], **William R. Heath**[3,4], **Prajwal Gurung**[5,6], **Kevin L. Legge**[2,6], **Chris J. Janse**[7], **Noah S. Butler**[1,6,8,*]

[1]Department of Microbiology and Immunology, University of Iowa, Iowa City, IA, USA

[2]Department of Pathology, University of Iowa, Iowa City, IA, USA

[3]Department of Microbiology and Immunology, Peter Doherty Institute for Infection and Immunity, University of Melbourne, VIC 3000, Australia

[4]ARC Centre of Excellence in Advanced Molecular Imaging, University of Melbourne, Parkville, VIC 3010, Australia

[5]Department of Internal Medicine, University of Iowa, Iowa City, IA, USA

[6]Interdisciplinary Graduate Program in Immunology, University of Iowa, Iowa City, IA, USA

[7]Leiden Malaria Research Group, Centre of Infectious Diseases, Leiden University Medical Centre, Leiden 233 ZA, the Netherlands

[8]Lead contact

SUMMARY

During acute malaria, most individuals mount robust inflammatory responses that limit parasite burden. However, long-lived sterilizing anti-malarial memory responses are not efficiently induced, even following repeated *Plasmodium* exposures. Using multiple *Plasmodium* species, genetically modified parasites, and combinations of host genetic and pharmacologic approaches, we find that the deposition of the malarial pigment hemozoin directly limits the abundance and capacity of conventional type 1 dendritic cells to prime helper T cell responses. Hemozoin-

*Correspondence: noah-butler@uiowa.edu.

AUTHOR CONTRIBUTIONS

A.D.P. designed and conducted the experiments, analyzed the data, generated figures, and wrote the manuscript. P.V.S. provided technical assistance. D.F.-R., W.R.H., and P.G. provided reagents and dendritic cell and inflammasome expertise. Z.R.Z. and K.L.L. provided assistance with dendritic cell functional analyses. C.J.J. provided mutant *P. berghei* parasites. N.S.B. edited the manuscript and supervised the studies.

SUPPLEMENTAL INFORMATION

Supplemental information can be found online at https://doi.org/10.1016/j.celrep.2021.109586.

INCLUSION AND DIVERSITY

We worked to ensure sex balance in the selection of non-human subjects. One or more of the authors of this paper self-identifies as an underrepresented ethnic minority in science. One or more of the authors of this paper self-identifies as a member of the LGBTQ+ community. One or more of the authors of this paper received support from a program designed to increase minority representation in science.

DECLARATION OF INTERESTS

The authors declare no competing interests.

induced dendritic cell dysfunction results in aberrant *Plasmodium*-specific CD4 T follicular helper cell differentiation, which constrains memory B cell and long-lived plasma cell formation. Mechanistically, we identify that dendritic cell-intrinsic NLRP3 inflammasome activation reduces conventional type 1 dendritic cell abundance, phagocytosis, and T cell priming functions *in vivo*. These data identify biological consequences of hemozoin deposition during malaria and highlight the capacity of the malarial pigment to program immune evasion during the earliest events following an initial *Plasmodium* exposure.

Graphical abstract

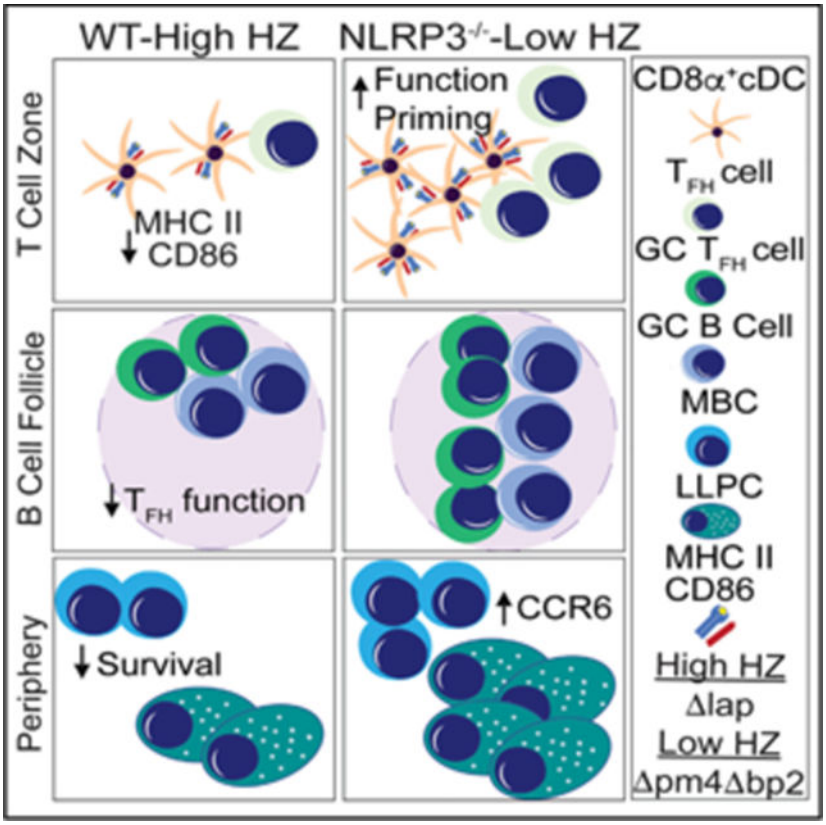

In brief

Using genetic, chimeric, and pharmacologic approaches, Pack et al. demonstrate that the parasite-derived crystal hemozoin erodes conventional CD8α$^+$ type 1 dendritic cell (cDC1) abundance and function in an NLRP3 inflammasome-dependent manner, which results in reduced CD4$^+$ T follicular helper cell differentiation and impaired anti-*Plasmodium* humoral immunity.

INTRODUCTION

Nearly half of the world's population lives in areas endemic to the disease syndrome malaria, which is caused by infection with protozoan parasites of the genus *Plasmodium*. Children under the age of 5 account for two-thirds of all malaria-associated mortality (WHO, 2019). Repeated parasite infections generally fail to elicit sterilizing immunity,

even following years of exposure among those living in regions of intense *Plasmodium* transmission (Tran et al., 2013). The emergence of parasite resistance to front-line antimalarial drugs (Das et al., 2018), coupled with the limited capacity of existing vaccines to elicit protection in endemic populations (Mensah et al., 2016; Rts, 2015), underscores the rationale for continued efforts to close knowledge gaps regarding the mechanisms, whether host or parasite associated, that restrict the development of durable, protective immune memory responses.

Following an initial *Plasmodium* infection and asymptomatic replication of parasites in the liver, schizont-induced rupture of parasite-infected red blood cells (pRBCs) liberates both host- and parasite-derived factors, including host RBC membranes, parasite antigens, and nucleic acids, that are recognized and often captured by host phagocytes. These stimuli rapidly induce the activation of macrophages and dendritic cells (DCs) that produce reactive oxygen and nitrogen species (Chua et al., 2013; Ranjan et al., 2016; Sobolewski et al., 2005; Sponaas et al., 2009), which are believed to limit infection intensity prior to the induction and orchestration of anti-*Plasmodium* cellular and humoral immunity. Phagocytes are also responsible, in part, for the production of high levels of proinflammatory cytokines such as interleukin (IL)-1β, IL-12, and interferon (IFN)-γ that both amplify the activation and recruitment of additional effector immune cells (Leisewitz et al., 2004; Perry et al., 2005; Wykes et al., 2007) and contribute to clinical malarial disease syndrome (deWalick et al., 2007). In addition to initiating and amplifying host immunity, DCs also contribute to the initiation of T follicular helper (T_{FH}) cell differentiation via MHC II-restricted antigen presentation and costimulation (Choi et al., 2011; Langenkamp et al., 2000). T_{FH} populations, in turn, are critical for orchestrating protective pathogen-specific humoral responses and deficiencies in anti-malarial humoral immunity have been linked to altered T_{FH} development and function (Hansen et al., 2017; Ryg-Cornejo et al., 2016; Zander et al., 2016; Zander et al., 2015). Whether DCs are distinctly programmed during *Plasmodium* blood-stage infection such that they inefficiently support the development of anti-*Plasmodium* T_{FH} responses and humoral immunity is not well defined.

During either *in vivo* blood-stage infection or following direct *in vitro* incubation with pRBCs, DCs exhibit an atypical maturation phenotype (Elliott et al., 2007; Götz et al., 2017; Urban et al., 1999), as well as reduced responsiveness to LPS stimulation and impaired capacity to initiate heterologous immune responses during an active *Plasmodium* infection (Lundie et al., 2010; Millington et al., 2006). Compared to DCs from uninfected subjects, myeloid DCs isolated from the peripheral blood of *P. falciparum* exposed individuals expressed lower levels of CD80, CD86, and HLA-DR following *in vitro* stimulation with blood-stage parasites (Turner et al., 2021). *In vitro* incubation of DCs with intact and dissociated pRBCs, along with RBC ghosts (membranes), identified that hemozoin, a crystalized parasite-derived hemoglobin degradation byproduct and NLRP3 inflammasome and CLEC12A agonist (Kalantari et al., 2014; Raulf et al., 2019; Shio et al., 2009), can alter DC function (Schwarzer et al., 1998; Skorokhod et al., 2004). However, whether modulating hemozoin levels in the context of natural *Plasmodium* blood-stage infection directly impacts DC-dependent development of anti-*Plasmodium* humoral responses has not been investigated.

In this report, we combined genetic, chimeric, and pharmacologic approaches to interrogate whether hemozoin exposure during experimental malaria impacts immune programming and the development of protective anti-*Plasmodium* humoral immune memory responses. Using both genetically modified *Plasmodium berghei* (*Pb*) parasites engineered to produce 10-fold lower levels of hemozoin (Lin et al., 2015) and wild-type *P. yoelii* infection of NLRP3-deficient mice, we show that hemozoin-induced, DC-intrinsic NLRP3-mediated inflammasome activation compromises T_{FH} differentiation, which in turn limits anti-*Plasmodium* memory B cell and the long-lived plasma cell responses and protective humoral immunity against malaria.

RESULTS

Durable anti-*Plasmodium* humoral immunity is compromised by hemozoin

To address whether hemozoin formation and deposition influences the generation of durable anti-malarial immunity, we established memory immune responses in wild-type C57BL/6 mice by infecting them with a genetically modified *Plasmodium berghei* ANKA variant lacking the aspartic proteases plasmepsin 4 and berghepain-2 (Δ*pm4*Δ*bp2*), genes that are necessary for efficient degradation of hemoglobin and crystallization of hemozoin (Lin et al., 2015; Spaccapelo et al., 2010). Mature schizonts of Δ*pm4*Δ*bp2* parasites produce less hemozoin compared to wild-type (WT) *P. berghei* ANKA parasites with 50% reductions in hemozoin accumulation within the spleen as early as day 5 post-infection (p.i.) (Figure S1A). Because Δ*pm4*Δ*bp2* parasites also exhibit reduced growth and replication *in vivo* compared to WT Pb ANKA parasites (Lin et al., 2015), other groups of mice were infected with a comparison mutant of growth-attenuated *P. berghei* lacking leucyl aminopeptidase (Δ*lap*), a mutant that is not impaired in hemozoin production (Lin et al., 2015) but exhibits growth and clearance kinetics that are equivalent to Δ*pm4*Δ*bp2* parasites (Figure S1B). These genetically modified parasites enabled us to directly address the *in vivo* role of hemozoin and avoid major caveats associated with injection of exogenous hemozoin, including the form (i.e., synthetic or natural), site of accumulation, and dose (Pham et al., 2021). Sixty days after the initial infection with either Δ*lap* or Δ*pm4*Δ*bp2* parasites, we challenged both groups of mice with WT (virulent) *P. berghei* ANKA parasites engineered to express the fusion protein GFP-Luciferase (*Pb*-ANKA-Luc) (Figure 1A). Compared to Δ*lap*-immune mice, Δ*pm4*Δ*bp2*-immune mice exposed to lower levels of hemozoin during primary infection exhibited reduced parasitemia (Figure 1B) and total parasite biomass luminescence (Figure 1C) across all time points examined and whole-body bioluminescent imaging revealed substantial *Pb*-ANKA-Luc tissue accumulation in Δ*lap*-immune mice that was absent in Δ*pm4*Δ*bp2*-immune mice (Figure 1C). Δ*pm4*Δ*bp2*-immune mice also exhibited 100% survival following WT *Pb*-ANKA-Luc challenge (Figure 1D).

Because Δ*pm4*Δ*bp2*-immune mice exhibited enhanced control of WT Pb-ANKA as early as days 3–4 post-challenge, relative to Δ*lap*-immune mice (Figure 1B), we further posited that the observed resistance to virulent *Pb*-ANKA-Luc challenge could be attributed to pre-existing, protective anti-*Plasmodium* antibodies. Consistent with this hypothesis, passive transfer of purified immunoglobulin G (IgG) from Δ*pm4*Δ*bp2*-immune donors to WT *Pb*-ANKA-infected recipient mice (Figure 1E) transiently resulted in a 75% reduction

in parasitemia, compared to transfer of an equivalent amount of purified IgG from Δ*lap*-immune donors (Figure 1F), although immune IgG transfer was not sufficient to protect recipients beyond the first week (Figure S1C). Strikingly, antibody titers directed against the 19 kDa fragment of Merozoite Surface Protein 1 ($MSP1_{19}$), an immunodominant and protective blood-stage antigen (John et al., 2004; O'Donnell et al., 2001; Terrientes et al., 1994), were not detectably different between Δ*lap* and Δ*pm4*Δ*bp2*-immune mice (Figure S1D), and we found no significant alterations in the total IgG antibody avidity index or isotype class distributions (Figures S1E and S1F). Nevertheless, our passive transfer data are consistent with an enhanced long-lived antibody response in Δ*pm4*Δ*bp2*-immune mice, compared to Δ*lap*-immune mice, which may be reflected by either quantitative or qualitative (specificity and functional) shifts that register below the sensitivity of these assays.

Secreted anti-*Plasmodium* antibodies that are present 60 days p.i. likely derive from long-lived plasma cells (LLPCs) that often reside in the bone marrow (Lightman et al., 2019). Given the enhanced protective capacity of Δ*pm4*Δ*bp2*-immune IgG, we quantified parasite-specific LLPC in the bone marrow during the memory phase. By day 40 p.i., we found approximately 2-fold greater numbers of $CD138^{hi}TACI^{hi}CD19^{lo}B220^{lo}$ mature resting LLPC (Pracht et al., 2017) (Figures 1G and 1H) and functional $MSP1_{19}$-specific IgG secreting cells (Figure 1I; Figure S1G) in the bone marrow of Δ*pm4*Δ*bp2*-immune mice, compared to Δ*lap*-immune mice. Thus, we next evaluated the kinetics of parasite-specific LLPC formation. As early as day 14 p.i., the frequency and number of splenic $CD38^{+}IgD^{neg}CD138^{hi}$ LLPC precursors expressing CXCR4, a chemokine receptor associated with bone marrow homing (Nie et al., 2004), was 30%–40% greater in Δ*pm4*Δ*bp2*-infected mice (Figures 1J and 1K). By day 28 p.i., the bone marrow of Δ*pm4*Δ*bp2*-immune mice presented with twice as many $CD38^{+}IgD^{neg}CD138^{hi}TACI^{hi}$ LLPC (Figure 1L) and $MSP1_{19}$-specific IgG-secreting cells (Figure 1M), compared to Δ*lap*-immune mice. Taken together, these data support that deposition of hemozoin during a primary blood-stage *Plasmodium* exposure impairs either the development or function of LLPC and durable anti-*Plasmodium* humoral responses.

Hemozoin compromises memory B cell responses

Given the deleterious effect of hemozoin on LLPC development and function following primary blood-stage infection, we additionally hypothesized that hemozoin may interfere with the development and function of memory B cell (MBC) populations. Consistent with this hypothesis, splenic $CD19^{+}CD38^{+}IgD^{neg}CD73^{+}CD95^{neg}$ MBC and $CD19^{+}CD38^{+}IgD^{neg}CD73^{+}CD80^{+}PD\text{-}L2^{+}$ MBC, with $CD80^{+}PD\text{-}L2^{+}$ defining those most capable of rapid antibody production (Zuccarino-Catania et al., 2014), were elevated 2-fold by day 30 p.i. in Δ*pm4*Δ*bp2*-immune mice, compared to Δ*lap*-immune mice (Figures 2A-2D). The chemokine receptor CCR6 is reported to enhance cell positioning within secondary lymphoid tissues for superior recall upon pathogen challenge (Elgueta et al., 2015; Suan et al., 2017) and by day 60 p.i., the frequency of splenic MBC cells expressing CCR6 were 2- to 3-fold greater in Δ*pm4*Δ*bp2*-immune mice, compared to Δ*lap*-immune mice (Figures 2E-2G). To interrogate functional MBC responses, we evaluated $MSP1_{19}$-specific serum antibody titers in Δ*pm4*Δ*bp2* and Δ*lap*-immune mice both prior to and 5 days after challenge with WT *Pb*-ANKA. In this short interval, increases in $MSP1_{19}$-specific,

isotype-switched IgG titers are most likely due to MBC activation and differentiation into plasma cells, rather than *de novo* humoral immune responses. Although Δ*pm4*Δ*bp2*-immune mice harbor 2-fold higher numbers of MBC (Figures 2A-2D), 5 days after challenge $MSP1_{19}$-specific IgG titers expanded by 10-fold, as compared to 3-fold in Δ*lap*-immune mice (Figure 2H). Together, these data suggest that recall functions of MBC are impaired by the presence and deposition of hemozoin.

CD4 T cell help and germinal center B cell responses are impaired by hemozoin

LLPC and MBC populations derive from germinal center (GC) B cell responses (Mesin et al., 2016; Weisel et al., 2016) and hemozoin deposition was associated with reduced LLPC and MBC development as early as days 14 and 30 p.i. in Δ*pm4*Δ*bp2*-infected mice, time points that encompass the peak of GC B cell responses following experimental *Plasmodium* (Krishnamurty et al., 2016; Vijay et al., 2020). Indeed, by day 14 p.i. the frequency and number of $CD95^{+}GL\text{-}7^{+}$ GC B cells were elevated by ~30% in Δ*pm4*Δ*bp2*-infected mice, compared to Δ*lap*-infected mice (Figures 3A and 3B). Because GC B cell responses depend on the presence and activity of T_{FH} cells (Kräutler et al., 2017), we next postulated that hemozoin impairs either the induction, stepwise differentiation, or function of T_{FH} populations. To test this hypothesis, we transferred *Plasmodium*-specific CD4 T cell receptor transgenic cells (PbTII [Fernandez-Ruiz et al., 2017]) to WT mice, infected recipients 1 day later with either Δ*pm4*Δ*bp2* or Δ*lap* parasites and then quantified both polyclonal, endogenous and PbTII CD4 T cells exhibiting characteristics of either mature $CXCR5^{hi}PD\text{-}1^{hi}$ GC-T_{FH} cells that localize to follicular GC reactions or their extrafollicular $CD150^{lo}CXCR5^{int}$ T_{FH} precursors (Choi et al., 2011; Crotty, 2014). By day 14 p.i., we found 30%–50% increases in the frequencies and numbers of both $CD150^{lo}CXCR5^{int}T_{FH}$ precursors (Figures 3C and 3D) and mature $CXCR5^{hi}PD\text{-}1^{hi}$ GC-T_{FH} subsets (Figures 3E and 3F) among PbTII cells in Δ*pm4*Δ*bp2*-infected mice, compared to PbTII cells in Δ*lap*-infected mice. We also observed 2-fold greater numbers of $CXCR5^{hi}PD\text{-}1^{hi}$ GC-T_{FH} cells among polyclonal endogenous CD4 T cells recovered from Δ*pm4*Δ*bp2*-infected mice (Figures 3G and 3H), supporting the view that this effect extends to the endogenous CD4 T cell receptor repertoire. Bcl-6 is a transcriptional repressor that is essential for T_{FH} differentiation and function (Hatzi et al., 2015) and $T\text{-}bet^{+}$ T_H1-like T_{FH} and $Foxp3^{+}$ T regulatory cells are reported to constrain anti-*Plasmodium* humoral immunity (Kurup et al., 2017; Obeng-Adjei et al., 2015). However, on 14 p.i., we identified only modestly reduced levels of T-bet and Foxp3, and equivalent expression levels of Bcl-6, in mature GC-T_{FH} cells recovered from Δ*pm4*Δ*bp2*-infected mice, compared to mature GC-T_{FH} cells recovered from Δ*lap*-infected animals (Figure 3I; Figure S2A). Despite these modest cell-intrinsic transcriptional differences, we additionally tested whether mature GC-T_{FH} cells recovered from Δ*pm4*Δ*bp2*-infected mice differed in their capacity to promote GC B cell differentiation. We sort-purified mature $CXCR5^{hi}PD\text{-}1^{hi}$GC-$T_{FH}$ from each group and co-cultured cells with an equivalent number with naive B cells for 5 days (Figure 3J). We observed significant increases in the proportions of B cells exhibiting a $CD95^{+}GL\text{-}7^{+}$ GC phenotype when cells were cultured with mature GC-T_{FH} recovered from Δ*pm4*Δ*bp2*-infected mice, compared to mature GC-T_{FH} cells recovered from Δ*lap*-infected mice (Figures 3K and 3L). Moreover, T_{FH} cells sort-purified on day 7 p.i. from the spleens of Δ*lap*-infected mice were also impaired in their capacity to drive GC responses following

transfer to *Tcra*$^{-/-}$ recipients, compared to T_{FH} recovered from Δ*pm4*Δ*bp2*-infected mice (Figures 3M-3P; Figures S2B-S2D). Together, these data support that the presence of elevated levels of hemozoin impairs the differentiation and cell-intrinsic function of T_{FH} cells with subsequent reductions in GC B cell responses.

Conventional DC functions are compromised by hemozoin

CD11c^{+}B220^{neg} conventional dendritic cells (cDCs), particularly the CD11b^{neg}CD8α^{+} conventional type 1 DC (cDC1) subset, are critical for initiating protective T cell responses against blood-stage *Plasmodium* infection (Fernandez-Ruiz et al., 2017; Voisine et al., 2010). Total CD11c^{+}B220^{neg} cDC numbers, phagocytic functions, and cytokine expression are reported to progressively decline during the course of experimental and clinical malaria, which has been described as immunoparalysis (Loughland et al., 2016; Lundie et al., 2010; Pinzon-Charry et al., 2013; Woodberry et al., 2012). Moreover, purified hemozoin can down-modulate DC reactivity following direct co-incubation *ex vivo* (Millington et al., 2006; Skorokhod et al., 2004). However, whether the deposition and/or accumulation of hemozoin specifically impairs either total cDC or cDC1 functions during blood-stage *Plasmodium* infection *in vivo* has not been directly tested. To investigate this, we examined cDC subset abundance, costimulatory receptor expression, and phagocytic function in Δ*pm4*Δ*bp2* and Δ*lap*-infected mice (representative gating, Figure S3A). As early as day 4 p.i., we found elevated numbers of CD11c^{+}B220^{neg} cDCs in Δ*pm4*Δ*bp2*-infected mice, compared to their Δ*lap*-infected counterparts (Figures 4A and 4B). These increases were primarily associated with elevated frequencies and numbers of CD11b^{neg}CD8α^{+} cDC1 in Δ*pm4*Δ*bp2*-infected mice (Figures 4C-4E) expressing elevated levels of MHCII (Figures 4F and 4G). Although expression of the costimulatory molecule CD80 was unaffected by hemozoin abundance (Figures 4H and 4I), CD86 expression was significantly increased on CD11b^{neg}CD8α^{+} cDC1 recovered from Δ*pm4*Δ*bp2*-infected mice (Figures 4J and 4K). Relative to cells from Δ*lap*-infected mice, similar frequencies of cDC1 from Δ*pm4*Δ*bp2*-infected mice exhibited the capacity to phagocytose fluorescent carboxylate beads and OVA protein, but the quantities of each phagocytosed reagent (gMFI) were significantly elevated (Figures 4L-4O). Enhanced cDC1 function was also observed in antigen processing, as CD11b^{neg}CD8α^{+} cDC1 DCs recovered from Δ*pm4*Δ*bp2*-infected mice exhibited more efficient ovalbumin (OVA) protein cleavage and endosomal accumulation, compared to cDC1 recovered from Δ*lap*-infected mice (Figures 4P and 4Q). Compromises in cDC antigen accumulation and processing and MHCII and costimulatory receptor expression were further magnified by the second week of primary infection in Δ*lap*-infected mice (Figures S3B-S3I). Of note, CD11b^{+}CD8α^{neg} cDC2 functions were also impacted by the abundance of hemozoin, although these impacts were more modest (Figures S3J-S3L). Finally, and despite the caveats associated with dose, schedule, and formulation, we also found that direct injection of synthetic hemozoin into Δ*pm4*Δ*bp2*-infected mice reversed the enhanced cDC1 abundance (Figures S4A-S4C), MHC II expression (Figures S4D and S4E), and antigen processing (Figures S4F and S4G). These data phenocopy parameters observed in Δ*lap*-infected mice and serve as an additional complementary approach to show that hemozoin impairs cDC1 functions during *Plasmodium* infection.

Hemozoin limits early CD4 T cell expansion and differentiation

Given the changes we observed in cDC number, phenotype, and function, we further tested whether hemozoin impaired the capacity of cDC to prime *Plasmodium*-specific CD4 T cells. PbTII activation and division, as evidenced by CTV dilution, was first evaluated on day 4 p.i., which corresponds to a time point matching our kinetic analyses of impaired cDC function (Figure 4) and the reported development of cDC immunoparalysis (Lundie et al., 2010). Consistent with our cDC phenotypic and functional analyses, reduced levels of hemozoin in Δ*pm4*Δ*bp2*-infected mice increased the capacity of antigen-presenting cells (APCs) to support parasite-specific T cell proliferation (Figure 5A). There were nearly 20% increases in the proportion of PbTII that proliferated and nearly 50% increases in the proportion of divided PbTII cells that differentiated into $CD150^{lo}CXCR5^{int}T_{FH}$ precursor cells (Figures 5B and 5C). APC:CD4 T cell interactions are also crucial for helper cell migration into the GC, and this transition is regulated in part by either the strength of TCR stimulation (Benson et al., 2015; Goenka et al., 2011; Moran et al., 2011; Zemmour et al., 2018) or dwell time with APC (González et al., 2005; Govern et al., 2010). To investigate these aspects of cDC function, we transferred Nur77-GFP PbTII reporter cells to both Δ*pm4*Δ*bp2* and Δ*lap*-infected mice and found that reduced levels of hemozoin in Δ*pm4*Δ*bp2*-infected mice significantly enhanced TCR stimulation strength (Figures 5D and 5E), which likely contributes to the expanded number and proportion of T_{FH} cells in Δ*pm4*Δ*bp2*-infected mice (Figure 3 and Figures 5B and 5C). In contrast to day 14 p.i. $CXCR5^{hi}PD\text{-}1^{hi}$ mature GC-T_{FH} (Figure 3I), we found elevated Bcl-6 expression among $CD150^{lo}CXCR5^{int}$ T_{FH} precursor cells on days 7 and 10 p.i. (Figure 5F) in mice exposed to reduced levels of hemozoin. Importantly, the skewing of CD4 T cells toward a GC T_{FH} fate in Δ*pm4*Δ*bp2*-infected mice was cDC intrinsic, as *ex vivo* co-culture of $GP_{66–77}$ peptide-pulsed cDCs isolated from Δ*pm4*Δ*bp2*-infected mice resulted in both enhanced proliferation (Figures 5G and 5H) and trending upregulation of PD-1 and CXCR5 by $GP_{66–77}$-specific TCR transgenic SMARTA CD4 T cells (Figures 5I and 5J). Notably, and similar to the cDC datasets, injection of synthetic hemozoin into Δ*pm4*Δ*bp2*-infected mice reversed the enhanced parasite-specific T_{FH} differentiation phenotypes (Figures S4H and S4I). Taken together, these data support that cDC are numerically and functionally compromised by hemozoin and this alters their capacity to optimally induce CD4 T cell responses and T_{FH} differentiation during blood-stage *Plasmodium* infection.

NLRP3 activation prevents the development of optimal T_{FH} and humoral responses

To interrogate the mechanisms by which hemozoin erodes cDC numbers and function, with subsequent impacts in T_{FH} cell development and humoral immunity, we focused on the NLRP3 inflammasome. *In vitro* data support that hemozoin engages and activates the NLRP3 inflammasome (Kalantari et al., 2014; Shio et al., 2009; Strangward et al., 2018), and we found that serum IL-1β levels were on average 75% lower in mice infected with Δ*pm4*Δ*bp2* parasites, compared to mice infected with Δ*lap* parasites (Figure S5A). Thus, we next tested whether the enhanced T_{FH} cell differentiation phenotypes we observe in Δ*pm4*Δ*bp2*-infected mice were formally linked to NLRP3 inflammasome activation. To do this, we first transferred WT PbTII CD4 T cells to both C57BL/6 (WT) and NLRP3 deficient (KO) mice and subsequently infected the recipients with either Δ*lap* or Δ*pm4*Δ*bp2* parasites. Consistent with our previous observations (Figure 3), we found

reduced frequencies of both PbTII CD150^{lo}CXCR5^{int} T_{FH} precursors and CXCR5^{hi}PD-1^{hi} mature GC-T_{FH} populations in Δ*lap*-infected WT mice, compared to Δ*pm4*Δ*bp2*-infected WT mice (Figure 6A, left panels). Strikingly, PbTII T_{FH} and GC-T_{FH} development in both Δ*lap*-infected NLRP3 KO mice and WT mice treated from days 0 to 6 p.i. with the NLRP3 inflammasome inhibitor MCC950 phenocopied PbTII T_{FH} differentiation in Δ*pm4*Δ*bp2*-infected WT mice (Figure 6A, right panels). NLRP3 activation also impaired the capacity of GC-T_{FH} to promote GC B cell responses, as mature GC-T_{FH} cells sort-purified from Δ*lap*-infected NLRP3 KO mice induced 2-fold greater numbers of GC B cell in *ex vivo* co-culture assays, compared to GC-T_{FH} cells recovered from Δ*lap*-infected WT mice (Figure 6B). In addition to the deleterious impact of NLPR3 activation on T_{FH} differentiation and function, the frequency and number of splenic GC B cells (Figures S5B and S5C) and CD95^{neg}CD73^{+}CD80^{+}PD-L2^{+} MBC (Figures 6C and 6D) were significantly decreased by either the presence of hemozoin or NLRP3 inflammasome activity.

To directly address whether hemozoin-mediated NLRP3 activation compromises long-term protective immunity *in vivo*, groups of both WT and NLRP3 KO mice were immunized with either Δ*pm4*Δ*bp2* or Δ*lap* parasites and then challenged with WT *Pb*-ANKA after 60 days (Figure 6E). Both WT and NLRP3 KO mice immunized with Δ*pm4*Δ*bp2* exhibited 100% survival and reduced parasite burden (Figures 6F, S5D, and S5E) through day 35 p.i. However, more than 75% of Δ*lap*-immune NLRP3 KO mice survived, compared to only 30% of Δ*lap*-immune WT mice (Figure 6F). We also found functional MBC recall antibody responses were substantially improved in Δ*pm4*Δ*bp2*-immune WT mice and Δ*lap*-immune NLRP3 KO mice, as evidenced by 38- and 169-fold boosts in parasite-specific IgG titers 5 days after *Pb*-ANKA challenge, respectively (Figure 6G), in contrast to the modest 7-fold boost in Δ*lap*-immune WT mice. Collectively, these experiments show that the infection of NLRP3-deficient mice with Δ*lap* parasites effectively phenocopies elevated GC-T_{FH} and MBC numbers and functions observed following infection of WT mice with Δ*pm4*Δ*bp2* parasites, further supporting that hemozoin-mediated NLRP3 activation impairs protective anti-*Plasmodium* humoral immunity.

Cell-intrinsic NLRP3 activation impairs cDC number and function

Our genetic and pharmacological approaches support that hemozoin-mediated NLRP3 inflammasome activation constrains T_{FH} dependent humoral immunity. To determine whether these phenotypes are mechanistically linked to cDC-intrinsic NLRP3 activity and confirm that our findings extend beyond study of the mutant *Pb* ANKA parasites, we first evaluated cDC numbers and functions and T_{FH} development in WT and NLRP3 deficient mice infected with *Plasmodium yoelii* parasites (Figure 7A). We observed that the total numbers of CD11b^{neg}CD8α^{+} cDC1 (Figures 7B and 7C), and their relative MHC II expression (Figure 7D) were significantly increased in the absence of NLRP3 activation. Moreover, the capacity of cDC1 from *P. yoelii*-infected mice to both phagocytose multiple carboxylate beads (gMFI) (Figure 7E) and functionally process and accumulate cleaved OVA protein (Figures 7F and 7G) was markedly enhanced in the absence of hemozoin-mediated NLRP3 inflammasome activation, which closely resembles our findings with the mutant *Pb* ANKA parasites (Figure 4). Both PbTII and polyclonal CD4 T cell responses were also skewed toward a more robust T_{FH} phenotype in *P. yoelii*-infected

NLRP3-deficient mice, compared to *P. yoelii*-infected WT mice (Figures 7H and 7I). Importantly, *P. yoelii*-immune NLRP3-deficient mice were substantially more resistant to challenge with WT *Pb* ANKA (Figures S6A-S6C), phenotypes that additionally associated with enhanced MBC recall function (Figure S6D). Together, these data provide additional support that NLRP3 activation compromises cDC function and results in suboptimal T_{FH} responses and protective humoral immunity.

Finally, to compare WT and NLRP3 KO cDC1 development and function in the same *Plasmodium*-infected host, we generated and infected WT:NLRP3 KO (50:50) mixed bone-marrow chimeras with Δ*lap* parasites (Figure 7J). Importantly, this approach controls for potential differences in parasite load, antigen, and inflammation in *Plasmodium*-infected WT and KO mice. Although only modest shifts in cDC1:cDC2 ratios were observed among NLRP3 KO cells (Figure 7K), we observed that NLRP3 KO cells exhibited significantly elevated MHC II expression among both total cDC and $CD11b^{neg}CD8\alpha^{+}$ cDC1 populations (Figures 7L and 7M), compared to WT cDC and cDC1 populations. These data provide direct *in vivo* evidence that hemozoin-mediated cDC-intrinsic NLRP3 activation, rather than extrinsic and environmental cues that include inflammatory cytokines, such as IL-1β, regulate the expression of MHC II. Consistent with these findings, NLRP3 KO $CD11b^{neg}CD8\alpha^{+}$ cDC1 exhibited significantly enhanced phagocytotic (Figure 7N) and protein processing functions (Figures 7O and 7P), compared to WT cDC1 recovered from the same *Plasmodium* infection environment. Last, to complement these genetic studies and confirm that early NLRP3 activation leads to impaired humoral immunity, we treated *Δlap*-infected WT mice with MCC950 during the initial stages of DC activation and CD4 T cell priming (days 0 to 6 p.i.) and measured the development of $MSP1_{19}$-specific plasma cells. Pharmacologic inhibition of NLRP3 inflammasome activity resulted in 2-fold greater numbers of parasite-specific plasma cells by day 28 p.i. (Figures 7Q-7S). Altogether, our data provide direct *in vivo* evidence that hemozoin-mediated inflammasome activation during an initial blood-stage *Plasmodium* exposure limits cDC1 numbers and functions, which in turn impairs the development of protective anti-*Plasmodium* cellular and humoral immunity.

DISCUSSION

The adaptive immune response elicited by *Plasmodium* infection is robust, but the resilience of humoral memory populations is suboptimal. Waning immune-mediated resistance to malarial disease in individuals who emigrate from endemic areas and the failure of vaccines in endemic populations highlight that new mechanistic understanding of why humoral responses following *Plasmodium* exposure are suboptimal remains a priority. Our study revealed that these defects may be programmed early after an initial *Plasmodium* exposure via hemozoin-mediated, NLRP3 inflammasome-dependent impacts on the cDC compartment with significant reductions in phagocytosis, antigen processing, and MHC II expression occurring as early as day 4 p.i. We further linked these cDC re-programming events to impairments in the stepwise differentiation of T_{FH}, which resulted in reduced GC B cell responses and lower numbers of MBC and LLPC capable of producing protective, anti-parasite antibodies. Further investigation supported that humoral memory is suppressed by DC-intrinsic inflammasome activation. Importantly, hemozoin-induced NLRP3 activation

limited humoral immunity irrespective of the strain of parasites (*P. yoelii* or *P. berghei* ANKA) used to initiate cDC reprogramming, suggesting that sustained hemozoin-induced compromise of $CD8\alpha^+$ cDC numbers and function may be a conserved pathophysiologic feature of blood-stage *Plasmodium* infection.

Despite the genetic and life-cycle complexity of *Plasmodium* parasites, hemozoin is currently the only described malaria-associated NLRP3 inflammasome agonist. The capacity for inflammasome activation to alter cDC gene expression and phenotype has been evaluated *ex vivo*, but studies designed to evaluate the contribution of DC-intrinsic inflammasome activation during vaccination and infection are limited. A recent report showed that inflammasome activation during *Salmonella* infection is detrimental to T cell priming and that reduced levels of inflammasome machinery limit splenic DCs from undergoing inflammasome-mediated pyroptosis (McDaniel et al., 2020). It was further reported that cDC activation by inflammasomes rarely occurs early during infection because of IRF4 and IRF8-mediated suppression of inflammasome genes, but this observation is not consistent with those from the *Plasmodium* field where robust expression of inflammasome genes and caspase 1 activation are observed following both rodent and human infection (Ataide et al., 2014). Indeed, the magnitude of inflammasome activation that occurs during the blood stage of *Plasmodium* infection is supported by high levels of serum IL-1β, which contribute to malarial symptoms that include fever, chills, and malaise. Deleterious functions for hemozoin during malaria are also suggested by strong correlations between hemozoin accumulation and severe clinical manifestations and inflammation in the central nervous system and placenta, where increased accumulation of monocytes and platelets can exacerbate disease (Hochman et al., 2016; Milner et al., 2013; Moore et al., 2004; Nguyen et al., 1995; Sarr et al., 2006). We found that reducing cDC exposure to hemozoin limited splenic IL-1β levels by day 10 p.i. and significantly increased DC maturation kinetics and function. Our *in vivo* studies showed that hemozoin-induced, NLRP3-dependent inflammasome activation impaired cDC phagocytosis, antigen processing, and expression of MHC II. Reported discrepancies between experimental studies of *ex vivo* and *in vivo* contributions of inflammasome activation and resultant programming of DC fate and function may be linked to the severity of malaria or virulence of specific species of *Plasmodium* parasites, as well as the tissue-specific deposition and abundance of hemozoin. Our complementary genetic, biochemical, and pharmacologic studies support that NLRP3 activation exerts a similarly deleterious impact on humoral immunity following either *P. yoelii* or *P. berghei* ANKA primary infections.

The functional defects we observed in cDC following hemozoin-mediated NLRP3 inflammasome activation were further linked to negative impacts on the *Plasmodium*-specific T cell response. T cell priming, the emergence of $CD150^{lo}CXCR5^{int}T_{FH}$ precursors, and the eventual differentiation of mature $CXCR5^{hi}PD\text{-}1^{hi}GC\text{-}T_{FH}$ cells were all reduced by hemozoin-mediated NLRP3 activation in cDC. Notably, alum is a well-documented NLRP3 agonist and adjuvant reported to promote the initiation of T cell and humoral responses. Alum's capacity to dissociate from vaccine components upon injection differs significantly from that of hemozoin, which is retained within the DCs. This difference may serve as one explanation for disparities in reported outcomes following examination of NLRP3-mediated DC function. Our high-resolution analyses revealed that, in the absence of NLRP3

activation, parasite-specific T cells exhibited evidence of enhanced TCR stimulation, which is reported to support increased CXCR5 expression and reinforce T_{FH} differentiation. Whether the presence of hemozoin and altered DC programming impairs a limited number of GC-T_{FH} functions or reduces the expression of multiple co-stimulatory molecules and cytokines is not currently known. Elucidation of the precise mechanisms by which hemozoin limits the capacity of cDC to promote the development of optimal GC-T_{FH} function remains of interest and will also be relevant to our understanding of how *Plasmodium* infection influences responses to either heterologous infection or vaccination.

Our results support the hypothesis that hemozoin and the associated programming of DC number and function contribute to suboptimal humoral responses following *Plasmodium* infection. During a blood-stage *Plasmodium* infection with reduced levels of hemozoin, enhancements in humoral immunity begin early in the spleen, where we observed a coordinated shift in $CXCR4^+CD138^+$ LLPC precursors and accumulation of mature LLPC in the bone marrow. Our data support a model wherein the abundance of LLPC or reactivation of memory B cells mediate protection from lethal parasite challenge, as opposed to either qualitative shifts in either the isotype or affinity of parasite-specific antibodies in mice with reduced hemozoin exposure. Limitations of our study include the sensitivity of assays used to probe the quantity, quality, and functions of secreted antibody responses, particularly in our studies showing enhanced survival yet equivalent immune memory baseline titers in NLRP3 KO mice and WT mice infected with Δ*pm4*Δ*bp2* parasites. Future molecular and biophysical studies designed to interrogate critical qualitative attributes and effector functions of the secreted antibody responses are warranted. Another notable aspect of our studies that we did not assess is whether hemozoin accumulation within the bone marrow impacts or erodes the maintenance of either vaccine-induced or pathogen-specific LLPC. The bone marrow serves as an infection reservoir for *P. vivax* parasites, and the presence of hemozoin in the bone marrow pushes the cytokine environment toward a more proinflammatory state (Lee et al., 2017). Understanding whether either inflammation or cytokine and chemokine perturbations contribute to reductions in the frequency of mature LLPC following infection with *Plasmodium* may shed light onto additional factors that restrain the quality and/or durability of anti-*Plasmodium* humoral responses.

STAR★METHODS

RESOURCE AVAILABILITY

Lead contact—Further information and requests for resources and reagents should be directed to and will be fulfilled by the Lead Contact, Noah Butler (noah-butler@uiowa.edu).

Materials availability

- This study did not generate unique reagents.

Data and code availability

- All data reported in this paper will be shared by the lead contact upon request.
- This study did not generate/analyze datasets or code.

- Any additional information required to reanalyze the data reported in this paper is available from the lead contact upon request.

EXPERIMENTAL MODEL AND SUBJECT DETAILS

Animals—C57BL/6 wild-type (CD45.2 and CD45.1), C57BL/6-Tg(Nr4a1-EGFP/cre)820Khog/J (Nur77^{GFP} Stock No. 016617) and *Nlrp3*^{tm1Bhk} (NLRP3 KO stock No. 021302) were either purchased from The Jackson Laboratory or acquired from colonies at the University of Iowa. For the generation of WT: NLRP3$^{-/-}$ chimeras, CD45.1 wild-type recipient mice were irradiated with 475 rads twice, separated by 4 h. Bone marrow cells from CD45.1 (C57BL/6) and CD45.2 (NLRP3 KO) were mixed 50:50 and 1×10^7 were injected i.v. Mice were maintained on a Uniprim diet (Envigo) for 2 weeks. Chimerism was assessed at 8 weeks post-irradiation. Age and sex-matched mice between 6 and 13 weeks were used for all experiments. Ethics oversight for animal use was provided by The University of Iowa IACUC.

Parasite strains and infections—Two wild-type *P. berghei* ANKA parasite lines were used: the *Pb*-ANKA line, obtained from MR4 (American Type Culture Collection) and the reporter, reference *P. berghei* ANKA line 676m1cl1 (*Pb*-ANKA-Luc), which constitutively express GFP and luciferase that was obtained through BEI Resources (MRA-868) and was contributed by Chris J. Janse and Andrew P. Waters. The *Plasmodium berghei* ANKA mutants Δ*pm4*Δ*bp2* and Δ*lap* have been described in Lin et al. (2015) and were obtained from Dr. Chris Janse (Leiden University Medical Center, LUMC, the Netherlands). *P. yoelii* (clone 17XNL) were obtained from the Malaria Research and Reference Reagent Resource Center (MR4, American Type Culture Collection). All parasite lines were maintained by passage in NIH Swiss Webster mice. Primary infections were initiated by an intravenous (IV) transfer of 1 *× 10^6 parasitized red blood cells (RBCs) derived from an infected donor mouse. Challenge of mice with virulent *Pb*-ANKA or *Pb*-ANKA-luc were initiated by intravenous (IV) injection of 5×10^6 donor-derived parasitized RBCs.

Quantification of parasite biomass—Percentage of infected RBC was monitored in tail blood samples by flow cytometric analysis of the frequency of Hoechst$^+$ Diethydiumbromide$^+$Ter119$^+$CD45^{neg} cells (Malleret et al., 2011). Parasite loads, quantified as total flux (p/s/cm^2/sr), following IP injection of 250 μg of D-luciferin (Promega) were determined using an IVIS Lumina S5 and Living Image software (Perkin Elmer).

Treatments—Synthetic hemozoin (sHZ) (InvivoGen; 750 μg in PBS) was injected every second day IV (tail vein). MCC950 (Sigma, 250 μg in PBS) was administered via intraperitoneal (IP) injection every 2 days beginning at the time of infection.

METHOD DETAILS

Immune cell phenotyping—For analysis of splenic cells, single cell suspensions were generated by forcing mouse spleens through a 70 μm mesh. For experiments enumerating cDC subsets, spleens were incubated with collagenase IV (100 U/mL) and DNase I (10 μg/mL) for 30 mins at 37°C prior to preparation of single cell suspensions. RBC were lysed prior to Fc receptor blockade (CD16/32-clone 2.4G2) in FACS buffer (PBS+ 0.09%

sodium azide + 2% FCS) for 15 min at 4°C prior to surface staining. For identifying T_{FH} like cells, cells were stained with purified rat anti-mouse CXCR5 (BD Biosciences) in T_{FH} staining buffer (PBS+ 0.09% sodium azide + 2% FCS+ 0.05% BSA+ 2% mouse serum) for 1h at 4 °C. Cells were washed then stained with biotin-conjugated AffiniPure Goat anti-rat IgG (H+L) (Jackson Immunoresearch) in T_{FH} buffer for 30 min. Cells were then washed and surfaced stained in an antibody cocktail containing (Anti-CD4, -PD-1, -CD150, -CD11a, -CD44, streptavidin) for at least 30 min at 4°C. Anti-Bcl-6, -T-bet and -Foxp3 (BioLegend) transcription factor staining was performed using the Foxp3 Staining Kit per manufacturer's protocol (BD Biosciences). For B cell staining, cells were surface stained in FACS buffer for at least 30 min in the following cocktail solution containing anti-CD19, -B220, -CD267, -CD138, -CD38 (BioLegend), -CD95 (BD PharMingen), -IgD and -CXCR4 (BioLegend) to identify plasma cells, while a cocktail of anti-CD19, -B220, -CD38, -CD80, -CD273, -CD73, -IgD, -CCR6 (BioLegend) was used to identify memory B cells. cDCs were identified using a surface stain mix containing Anti-CD8, -F4/80, -CD80, -CD86, -CD19, -B220, -CD11c (BioLegend) and anti-CD11b and MHC II (Thermofisher) following Fc-block for 10 mins at 4°C.

Standard and antibody affinity ELISA—For standard ELISA, Nunc Immunosorb Plates were coated with 1 μg/mL of recombinant MSP19 overnight at 4°C. Plates were blocked for 2h at RT with PBS+2.5%BSA+ 2%FCS prior to addition of serially diluted sera and incubation overnight at 4°C. Wells were washed with PBS + 0.05% Tween20 prior to incubation with HRP conjugated anti-mouse IgG for 2h at RT. For affinity ELISA, after plates were coated overnight as described above, plates were washed with PBS-Tween prior to blocking with PBS+1% BSA+0.05% Tween for 1h at 37 °C. Diluted serum was incubated for 2h at RT in buffer (2.5% BSA+5% FCS in PBS). Wells were washed extensively with PBS+Tween20 prior to addition of diluted ammonium thiocyanate and incubation for 15 minutes. Wells were washed prior to incubation with HRP conjugated anti-mouse IgG for 1h at 37°C. All plates were reacted with SureBlue TMB Peroxidase and TMB Stop Solution (Sera Care) prior to absorbance measurement at an OD of 450 nm using a plate reader (Biotek). The concentration of serum IL-1β was assessed using an IL-1β LEGENDplex immunoassay (Biolegend) according to the manufacturer's protocol.

ELISPOT—White plates (Nunc MaxiSorp) were coated with 1 μg/mL of recombinant MSP-19 diluted in 0.1M Na_2HPO_4 binding solution and incubated overnight at 4°C. Plates were washed with PBS and blocked for 2h at RT with 10% FCS in RPMI 1640. Bone marrow cells were diluted serially in 10% FCS in RPMI 1640 and incubated for 18 h at 37 °C with 5% CO_2. Plates were thoroughly washed then incubated with HRP-conjugated anti-mouse IgG in PBS+5% FCS overnight at 4 °C. Spots were then developed with 3-amino-9-ethylcarbazole.

IgG purification—The method for IgG purification from immune serum using Protein G Sepharose4 Fast Flow columns was adapted from manufacturer's protocol and Akter et al. (Akter et al., 2019). Briefly, following column equilibration with binding buffer (20 mM sodium phosphate), diluted serum (1:4) was ran over column and flow-through was collected prior to complex elution. IgG was eluted from the column using 0.1M glycine+0.01%

sodium azide and the pH was neutralized using 1M Tris-HCl. Amicon Ultra-4 Membrane Units were used for buffer exchange to PBS.

CTV labeling of T cells—CTV labeled CD4+ T cells were prepared according to manufacturer's protocol (Invitrogen) with minor protocol modification. Splenocytes were washed and suspended in serum free media supplemented 1:1000 with Cell Trace Violet. Cells were incubated at 37°C for 20 min prior to dilution with RPMI 1640+10% FCS and incubation for 5 mins. Cells were pelleted and incubated again for 5 mins with RPMI 1640+10% FCS at 37°C prior to surface staining.

***Ex vivo* cultures—**GC-T_{FH} (CXCR5^{hi}PD-1^{hi}) were sort purified from Δ*pm4*Δ*bp2*- and Δ*lap*-infected mice on day 14 p.i. and suspended in IMDM+10% FCS. Naive B cells, enriched from naive mice using a B cell Isolation Kit (Miltenyi Biotec), were mixed with GC-T_{FH} at a 1:1 ratio and co-incubated for 5 days at 37°C with 5% CO_2. Cell cultures were supplemented with anti-IgM (5 μg/mL) (Jackson Immunoresearch) and anti-CD3 (5 μg/mL) (Biolegend). For cDC-T cell cultures, magnetically enriched cDCs were pulsed with 1 nM of GP-66 for 1h, washed, and incubated at a 1:10 ratio with CTV-labeled SMARTA cells for 4 days.

Phagocytosis assays—To examine the phagocytic capacity of cDC, splenocyte suspensions were incubated with Fluoresbrite carboxylate microsphere YG (0.5 μm-Polysciences) at a ratio of 1:100 microspheres/cell or in 25 μg/mL solution OVA-488 (Molecular Probes) for 1h at 37°C. To assess antigen processing by cDC, splenocytes were incubated in a 25 μg/mL solution of DQ-OVA (Molecular Probes) for 1h at 37°C. Cells were then stained with Fc-block for 10 mins at 4°C prior to surface staining.

QUANTIFICATION AND STATISTICAL ANALYSIS

Data centers in summary data graphs represent the mean. Data dispersion and tests of statistical significance are detailed in the figure legends. Graphs were generated and statistical analyses were performed using Prism Graphpad 9 software (GraphPad Software). For analyses comparing only two groups, Mann-Whitney non-parametric tests were used to determine p value. For comparison of 3 or more groups, Dunn's test for nonparametric multiple comparisons were employed and adjusted P values are reported. Details can be found in respective figure legends.

Supplementary Material

Refer to Web version on PubMed Central for supplementary material.

ACKNOWLEDGMENTS

The authors acknowledge the late Shahid M. Khan (University of Leiden) for his contributions to generating and characterizing the mutant parasites used throughout this study. We also thank members of the Butler lab for thoughtful discussions. The research reported in this publication was supported by the NCI (grant number P30CA086862) and the National Center for Research Resources of the NIH (grant number S10OD016199). A.D.P. was supported by the NIH (grant number T32AI007511). P.G. was supported by the NIH (grant number AI148904). Z.R.Z. was supported by the NIH (grant number T32AI007260). K.L.L. was supported by the NIH (grant numbers AI141196 and AI127565). W.R.H. was supported by the Australian Research Council (grant number

CE140100011) and the National Health and Medical Research Council (NHMRC; grant numbers 1113293 and 1154457). D.F-R. was supported by the National Health and Medical Research Council (grant number 1139486). N.S.B. was supported by the NIH (grant numbers AI125446 and AI127481).

REFERENCES

Akter J, Khoury DS, Aogo R, Lansink LIM, SheelaNair A, Thomas BS, Laohamonthonkul P, Pernold CPS, Dixon MWA, Soon MSF, et al. (2019). Plasmodium-specific antibodies block in vivo parasite growth without clearing infected red blood cells. PLoS Pathog. 15, e1007599. [PubMed: 30811498]

Ataide MA, Andrade WA, Zamboni DS, Wang D, Souza Mdo.C., Franklin BS, Elian S, Martins FS, Pereira D, Reed G, et al. (2014). Malaria-induced NLRP12/NLRP3-dependent caspase-1 activation mediates inflammation and hypersensitivity to bacterial superinfection. PLoS Pathog. 10, e1003885. [PubMed: 24453977]

Benson RA, MacLeod MK, Hale BG, Patakas A, Garside P, and Brewer JM (2015). Antigen presentation kinetics control T cell/dendritic cell interactions and follicular helper T cell generation in vivo. eLife 4, e06994.

Choi YS, Kageyama R, Eto D, Escobar TC, Johnston RJ, Monticelli L, Lao C, and Crotty S (2011). ICOS receptor instructs T follicular helper cell versus effector cell differentiation via induction of the transcriptional repressor Bcl6. Immunity 34, 932–946. [PubMed: 21636296]

Chua CL, Brown G, Hamilton JA, Rogerson S, and Boeuf P (2013). Monocytes and macrophages in malaria: protection or pathology? Trends Parasitol. 29, 26–34. [PubMed: 23142189]

Crotty S (2014). T follicular helper cell differentiation, function, and roles in disease. Immunity 41, 529–542. [PubMed: 25367570]

Das S, Saha B, Hati AK, and Roy S (2018). Evidence of Artemisinin-Resistant Plasmodium falciparum Malaria in Eastern India. N. Engl. J. Med 379, 1962–1964. [PubMed: 30428283]

deWalick S, Amante FH, McSweeney KA, Randall LM, Stanley AC, Haque A, Kuns RD, MacDonald KP, Hill GR, and Engwerda CR (2007). Cutting edge: conventional dendritic cells are the critical APC required for the induction of experimental cerebral malaria. J. Immunol 178, 6033–6037. [PubMed: 17475826]

Elgueta R, Marks E, Nowak E, Menezes S, Benson M, Raman VS, Ortiz C, O'Connell S, Hess H, Lord GM, and Noelle R (2015). CCR6-dependent positioning of memory B cells is essential for their ability to mount a recall response to antigen. J. Immunol 194, 505–513. [PubMed: 25505290]

Elliott SR, Spurck TP, Dodin JM, Maier AG, Voss TS, Yosaatmadja F, Payne PD, McFadden GI, Cowman AF, Rogerson SJ, et al. (2007). Inhibition of dendritic cell maturation by malaria is dose dependent and does not require Plasmodium falciparum erythrocyte membrane protein 1. Infect. Immun 75, 3621–3632. [PubMed: 17470539]

Fernandez-Ruiz D, Lau LS, Ghazanfari N, Jones CM, Ng WY, Davey GM, Berthold D, Holz L, Kato Y, Enders MH, et al. (2017). Development of a Novel $CD4^+$ TCR Transgenic Line That Reveals a Dominant Role for $CD8^+$ Dendritic Cells and CD40 Signaling in the Generation of Helper and CTL Responses to Blood-Stage Malaria. J. Immunol 199, 4165–4179. [PubMed: 29084838]

Goenka R, Barnett LG, Silver JS, O'Neill PJ, Hunter CA, Cancro MP, and Laufer TM (2011). Cutting edge: dendritic cell-restricted antigen presentation initiates the follicular helper T cell program but cannot complete ultimate effector differentiation. J. Immunol 187, 1091–1095. [PubMed: 21715693]

González PA, Carreño LJ, Coombs D, Mora JE, Palmieri E, Goldstein B, Nathenson SG, and Kalergis AM (2005). T cell receptor binding kinetics required for T cell activation depend on the density of cognate ligand on the antigen-presenting cell. Proc. Natl. Acad. Sci. USA 102, 4824–4829. [PubMed: 15772168]

Götz A, Tang MS, Ty MC, Arama C, Ongoiba A, Doumtabe D, Traore B, Crompton PD, Loke P, and Rodriguez A (2017). Atypical activation of dendritic cells by *Plasmodium falciparum*. Proc. Natl. Acad. Sci. USA 114, E10568–E10577. [PubMed: 29162686]

Govern CC, Paczosa MK, Chakraborty AK, and Huseby ES (2010). Fast on-rates allow short dwell time ligands to activate T cells. Proc. Natl. Acad. Sci. USA 107, 8724–8729. [PubMed: 20421471]

Hansen DS, Obeng-Adjei N, Ly A, Ioannidis LJ, and Crompton PD (2017). Emerging concepts in T follicular helper cell responses to malaria. Int. J. Parasitol 47, 105–110. [PubMed: 27866903]

Hatzi K, Nance JP, Kroenke MA, Bothwell M, Haddad EK, Melnick A, and Crotty S (2015). BCL6 orchestrates Tfh cell differentiation via multiple distinct mechanisms. J. Exp. Med 212, 539–553. [PubMed: 25824819]

Hochman SE, Madaline TF, Wassmer SC, Mbale E, Choi N, Seydel KB, Whitten RO, Varughese J, Grau GE, Kamiza S, et al. (2016). Author Correction for Hochman et al., Fatal Pediatric Cerebral Malaria Is Associated with Intravascular Monocytes and Platelets That Are Increased with HIV Coinfection. mBiol. 7, 02068–02015.

John CC, O'Donnell RA, Sumba PO, Moormann AM, de Koning-Ward TF, King CL, Kazura JW, and Crabb BS (2004). Evidence that invasion-inhibitory antibodies specific for the 19-kDa fragment of merozoite surface protein-1 (MSP-1 19) can play a protective role against blood-stage Plasmodium falciparum infection in individuals in a malaria endemic area of Africa. J. Immunol 173, 666–672. [PubMed: 15210830]

Kalantari P, DeOliveira RB, Chan J, Corbett Y, Rathinam V, Stutz A, Latz E, Gazzinelli RT, Golenbock DT, and Fitzgerald KA (2014). Dual engagement of the NLRP3 and AIM2 inflammasomes by plasmodium-derived hemozoin and DNA during malaria. Cell Rep. 6, 196–210. [PubMed: 24388751]

Kräutler NJ, Suan D, Butt D, Bourne K, Hermes JR, Chan TD, Sundling C, Kaplan W, Schofield P, Jackson J, et al. (2017). Differentiation of germinal center B cells into plasma cells is initiated by high-affinity antigen and completed by Tfh cells. J. Exp. Med 214, 1259–1267. [PubMed: 28363897]

Krishnamurty AT, Thouvenel CD, Portugal S, Keitany GJ, Kim KS, Holder A, Crompton PD, Rawlings DJ, and Pepper M (2016). Somatically Hypermutated Plasmodium-Specific IgM(+) Memory B Cells Are Rapid, Plastic, Early Responders upon Malaria Rechallenge. Immunity 45, 402–414. [PubMed: 27473412]

Kurup SP, Obeng-Adjei N, Anthony SM, Traore B, Doumbo OK, Butler NS, Crompton PD, and Harty JT (2017). Regulatory T cells impede acute and long-term immunity to blood-stage malaria through CTLA-4. Nat. Med 23, 1220–1225. [PubMed: 28892065]

Langenkamp A, Messi M, Lanzavecchia A, and Sallusto F (2000). Kinetics of dendritic cell activation: impact on priming of TH1, TH2 and nonpolarized T cells. Nat. Immunol 1, 311–316. [PubMed: 11017102]

Lee MSJ, Maruyama K, Fujita Y, Konishi A, Lelliott PM, Itagaki S, Horii T, Lin JW, Khan SM, Kuroda E, et al. (2017). *Plasmodium* products persist in the bone marrow and promote chronic bone loss. Sci. Immunol 2, 2.

Leisewitz AL, Rockett KA, Gumede B, Jones M, Urban B, and Kwiatkowski DP (2004). Response of the splenic dendritic cell population to malaria infection. Infect. Immun 72, 4233–4239. [PubMed: 15213168]

Lightman SM, Utley A, and Lee KP (2019). Survival of Long-Lived Plasma Cells (LLPC): Piecing Together the Puzzle. Front. Immunol 10, 965. [PubMed: 31130955]

Lin JW, Spaccapelo R, Schwarzer E, Sajid M, Annoura T, Deroost K, Ravelli RBG, Aime E, Capuccini B, Mommaas-Kienhuis AM, et al. (2015). Replication of Plasmodium in reticulocytes can occur without hemozoin formation, resulting in chloroquine resistance. J. Exp. Med 212, 893–903. [PubMed: 25941254]

Loughland JR, Minigo G, Burel J, Tipping PE, Piera KA, Amante FH, Engwerda CR, Good MF, Doolan DL, Anstey NM, et al. (2016). Profoundly Reduced CD1c+ Myeloid Dendritic Cell HLA-DR and CD86 Expression and Increased Tumor Necrosis Factor Production in Experimental Human Blood-Stage Malaria Infection. Infect. Immun 84, 1403–1412. [PubMed: 26902728]

Lundie RJ, Young LJ, Davey GM, Villadangos JA, Carbone FR, Heath WR, and Crabb BS (2010). Blood-stage Plasmodium berghei infection leads to short-lived parasite-associated antigen presentation by dendritic cells. Eur. J. Immunol 40, 1674–1681. [PubMed: 20391433]

Malleret B, Claser C, Ong AS, Suwanarusk R, Sriprawat K, Howland SW, Russell B, Nosten F, and Rénia L (2011). A rapid and robust tri-color flow cytometry assay for monitoring malaria parasite development. Sci. Rep 1, 118. [PubMed: 22355635]

McDaniel MM, Kottyan LC, Singh H, and Pasare C (2020). Suppression of Inflammasome Activation by IRF8 and IRF4 in cDCs Is Critical for T Cell Priming. Cell Rep. 31, 107604. [PubMed: 32375053]

Mensah VA, Gueye A, Ndiaye M, Edwards NJ, Wright D, Anagnostou NA, Syll M, Ndaw A, Abiola A, Bliss C, et al.; MVVC group (2016). Safety, Immunogenicity and Efficacy of Prime-Boost Vaccination with ChAd63 and MVA Encoding ME-TRAP against Plasmodium falciparum Infection in Adults in Senegal. PLoS ONE 11, e0167951. [PubMed: 27978537]

Mesin L, Ersching J, and Victora GD (2016). Germinal Center B Cell Dynamics. Immunity 45, 471–482. [PubMed: 27653600]

Millington OR, Di Lorenzo C, Phillips RS, Garside P, and Brewer JM (2006). Suppression of adaptive immunity to heterologous antigens during Plasmodium infection through hemozoin-induced failure of dendritic cell function. J. Biol 5, 5. [PubMed: 16611373]

Milner D Jr., Factor R, Whitten R, Carr RA, Kamiza S, Pinkus G, Molyneux M, and Taylor T (2013). Pulmonary pathology in pediatric cerebral malaria. Hum. Pathol 44, 2719–2726. [PubMed: 24074535]

Moore JM, Chaisavaneeyakorn S, Perkins DJ, Othoro C, Otieno J, Nahlen BL, Shi YP, and Udhayakumar V (2004). Hemozoin differentially regulates proinflammatory cytokine production in human immunodeficiency virus-seropositive and -seronegative women with placental malaria. Infect. Immun 72, 7022–7029. [PubMed: 15557625]

Moran AE, Holzapfel KL, Xing Y, Cunningham NR, Maltzman JS, Punt J, and Hogquist KA (2011). T cell receptor signal strength in Treg and iNKT cell development demonstrated by a novel fluorescent reporter mouse. J. Exp. Med 208, 1279–1289. [PubMed: 21606508]

Nguyen PH, Day N, Pram TD, Ferguson DJ, and White NJ (1995). Intraleucocytic malaria pigment and prognosis in severe malaria. Trans. R. Soc. Trop. Med. Hyg 89, 200–204. [PubMed: 7778149]

Nie Y, Waite J, Brewer F, Sunshine MJ, Littman DR, and Zou YR (2004). The role of CXCR4 in maintaining peripheral B cell compartments and humoral immunity. J. Exp. Med 200, 1145–1156. [PubMed: 15520246]

O'Donnell RA, de Koning-Ward TF, Burt RA, Bockarie M, Reeder JC, Cowman AF, and Crabb BS (2001). Antibodies against merozoite surface protein (MSP)-1(19) are a major component of the invasion-inhibitory response in individuals immune to malaria. J. Exp. Med 193, 1403–1412. [PubMed: 11413195]

Obeng-Adjei N, Portugal S, Tran TM, Yazew TB, Skinner J, Li S, Jain A, Felgner PL, Doumbo OK, Kayentao K, et al. (2015). Circulating Th1-Cell-type Tfh Cells that Exhibit Impaired B Cell Help Are Preferentially Activated during Acute Malaria in Children. Cell Rep. 13, 425–439. [PubMed: 26440897]

Perry JA, Olver CS, Burnett RC, and Avery AC (2005). Cutting edge: the acquisition of TLR tolerance during malaria infection impacts T cell activation. J. Immunol 174, 5921–5925. [PubMed: 15879082]

Pham TT, Lamb TJ, Deroost K, Opdenakker G, and Van den Steen PE (2021). Hemozoin in Malarial Complications: More Questions Than Answers. Trends Parasitol. 37, 226–239. [PubMed: 33223096]

Pinzon-Charry A, Woodberry T, Kienzle V, McPhun V, Minigo G, Lampah DA, Kenangalem E, Engwerda C, López JA, Anstey NM, and Good MF (2013). Apoptosis and dysfunction of blood dendritic cells in patients with falciparum and vivax malaria. J. Exp. Med 210, 1635–1646. [PubMed: 23835848]

Pracht K, Meinzinger J, Daum P, Schulz SR, Reimer D, Hauke M, Roth E, Mielenz D, Berek C, Côrte-Real J, et al. (2017). A new staining protocol for detection of murine antibody-secreting plasma cell subsets by flow cytometry. Eur. J. Immunol 47, 1389–1392. [PubMed: 28608550]

Ranjan R, Karpurapu M, Rani A, Chishti AH, and Christman JW (2016). Hemozoin Regulates iNOS Expression by Modulating the Transcription Factor NF-κB in Macrophages. Biochem. Mol. Biol. J 2, 10. [PubMed: 27790644]

Raulf MK, Johannssen T, Matthiesen S, Neumann K, Hachenberg S, Mayer-Lambertz S, Steinbeis F, Hegermann J, Seeberger PH, Baumgärtner W, et al. (2019). The C-type Lectin Receptor CLEC12A Recognizes Plasmodial Hemozoin and Contributes to Cerebral Malaria Development. Cell Rep. 28, 30–38. [PubMed: 31269448]

RTS,S Clinical Trials Partnership (2015). Efficacy and safety of RTS,S/AS01 malaria vaccine with or without a booster dose in infants and children in Africa: final results of a phase 3, individually randomised, controlled trial. Lancet 386, 31–45. [PubMed: 25913272]

Ryg-Cornejo V, Ioannidis LJ, Ly A, Chiu CY, Tellier J, Hill DL, Preston SP, Pellegrini M, Yu D, Nutt SL, et al. (2016). Severe Malaria Infections Impair Germinal Center Responses by Inhibiting T Follicular Helper Cell Differentiation. Cell Rep. 14, 68–81. [PubMed: 26725120]

Sarr D, Marrama L, Gaye A, Dangou JM, Niang M, Mercereau-Puijalon O, Lehesran JY, and Jambou R (2006). High prevalence of placental malaria and low birth weight in Sahelian periurban area. Am. J. Trop. Med. Hyg 75, 171–177. [PubMed: 16837727]

Schwarzer E, Alessio M, Ulliers D, and Arese P (1998). Phagocytosis of the malarial pigment, hemozoin, impairs expression of major histocompatibility complex class II antigen, CD54, and CD11c in human monocytes. Infect. Immun 66, 1601–1606. [PubMed: 9529087]

Shio MT, Eisenbarth SC, Savaria M, Vinet AF, Bellemare MJ, Harder KW, Sutterwala FS, Bohle DS, Descoteaux A, Flavell RA, and Olivier M (2009). Malarial hemozoin activates the NLRP3 inflammasome through Lyn and Syk kinases. PLoS Pathog. 5, e1000559. [PubMed: 19696895]

Skorokhod OA, Alessio M, Mordmüller B, Arese P, and Schwarzer E (2004). Hemozoin (malarial pigment) inhibits differentiation and maturation of human monocyte-derived dendritic cells: a peroxisome proliferator-activated receptor-gamma-mediated effect. J. Immunol 173, 4066–4074. [PubMed: 15356156]

Sobolewski P, Gramaglia I, Frangos JA, Intaglietta M, and van der Heyde H (2005). Plasmodium berghei resists killing by reactive oxygen species. Infect. Immun 73, 6704–6710. [PubMed: 16177347]

Spaccapelo R, Janse CJ, Caterbi S, Franke-Fayard B, Bonilla JA, Syphard LM, Di Cristina M, Dottorini T, Savarino A, Cassone A, et al. (2010). Plasmepsin 4-deficient Plasmodium berghei are virulence attenuated and induce protective immunity against experimental malaria. Am. J. Pathol 176, 205–217. [PubMed: 20019192]

Sponaas AM, Freitas do Rosario AP, Voisine C, Mastelic B, Thompson J, Koernig S, Jarra W, Renia L, Mauduit M, Potocnik AJ, and Langhorne J (2009). Migrating monocytes recruited to the spleen play an important role in control of blood stage malaria. Blood 114, 5522–5531. [PubMed: 19837977]

Strangward P, Haley MJ, Albornoz MG, Barrington J, Shaw T, Dookie R, Zeef L, Baker SM, Winter E, Tzeng TC, et al. (2018). Targeting the IL33-NLRP3 axis improves therapy for experimental cerebral malaria. Proc. Natl. Acad. Sci. USA 115, 7404–7409. [PubMed: 29954866]

Suan D, Kräutler NJ, Maag JLV, Butt D, Bourne K, Hermes JR, Avery DT, Young C, Statham A, Elliott M, et al. (2017). CCR6 Defines Memory B Cell Precursors in Mouse and Human Germinal Centers, Revealing Light-Zone Location and Predominant Low Antigen Affinity. Immunity 47, 1142–1153.e4. [PubMed: 29262350]

Terrientes ZI, Kramer K, Herrera MA, and Chang SP (1994). Naturally acquired antibodies against the major merozoite surface coat protein (MSP-1) of Plasmodium falciparum acquired by residents in an endemic area of Colombia. Mem. Inst. Oswaldo Cruz 89 (Suppl 2), 55–61. [PubMed: 7565133]

Tran TM, Li S, Doumbo S, Doumtabe D, Huang CY, Dia S, Bathily A, Sangala J, Kone Y, Traore A, et al. (2013). An intensive longitudinal cohort study of Malian children and adults reveals no evidence of acquired immunity to Plasmodium falciparum infection. Clin. Infect. Dis 57, 40–47. [PubMed: 23487390]

Turner TC, Arama C, Ongoiba A, Doumbo S, Doumtabé D, Kayentao K, Skinner J, Li S, Traore B, Crompton PD, and Götz A (2021). Dendritic cell responses to Plasmodium falciparum in a malaria-endemic setting. Malar. J 20, 9. [PubMed: 33407502]

Urban BC, Ferguson DJ, Pain A, Willcox N, Plebanski M, Austyn JM, and Roberts DJ (1999). Plasmodium falciparum-infected erythrocytes modulate the maturation of dendritic cells. Nature 400, 73–77. [PubMed: 10403251]

Vijay R, Guthmiller JJ, Sturtz AJ, Surette FA, Rogers KJ, Sompallae RR, Li F, Pope RL, Chan JA, de Labastida Rivera F, et al. (2020). Infection-induced plasmablasts are a nutrient sink that impairs humoral immunity to malaria. Nat. Immunol 21, 790–801. [PubMed: 32424361]

Voisine C, Mastelic B, Sponaas AM, and Langhorne J (2010). Classical CD11c+ dendritic cells, not plasmacytoid dendritic cells, induce T cell responses to Plasmodium chabaudi malaria. Int. J. Parasitol 40, 711–719. [PubMed: 19968996]

Weisel FJ, Zuccarino-Catania GV, Chikina M, and Shlomchik MJ (2016). A Temporal Switch in the Germinal Center Determines Differential Output of Memory B and Plasma Cells. Immunity 44, 116–130. [PubMed: 26795247]

WHO (2019). World malaria report 2019 (WHO).

Woodberry T, Minigo G, Piera KA, Amante FH, Pinzon-Charry A, Good MF, Lopez JA, Engwerda CR, McCarthy JS, and Anstey NM (2012). Low-level Plasmodium falciparum blood-stage infection causes dendritic cell apoptosis and dysfunction in healthy volunteers. J. Infect. Dis 206, 333–340. [PubMed: 22615323]

Wykes MN, Liu XQ, Beattie L, Stanisic DI, Stacey KJ, Smyth MJ, Thomas R, and Good MF (2007). Plasmodium strain determines dendritic cell function essential for survival from malaria. PLoS Pathog. 3, e96. [PubMed: 17616976]

Zander RA, Obeng-Adjei N, Guthmiller JJ, Kulu DI, Li J, Ongoiba A, Traore B, Crompton PD, and Butler NS (2015). PD-1 Co-inhibitory and OX40 Co-stimulatory Crosstalk Regulates Helper T Cell Differentiation and Anti-Plasmodium Humoral Immunity. Cell Host Microbe 17, 628–641. [PubMed: 25891357]

Zander RA, Guthmiller JJ, Graham AC, Pope RL, Burke BE, Carr DJ, and Butler NS (2016). Type I Interferons Induce T Regulatory 1 Responses and Restrict Humoral Immunity during Experimental Malaria. PLoS Pathog. 12, e1005945. [PubMed: 27732671]

Zemmour D, Zilionis R, Kiner E, Klein AM, Mathis D, and Benoist C (2018). Single-cell gene expression reveals a landscape of regulatory T cell phenotypes shaped by the TCR. Nat. Immunol 19, 291–301. [PubMed: 29434354]

Zuccarino-Catania GV, Sadanand S, Weisel FJ, Tomayko MM, Meng H, Kleinstein SH, Good-Jacobson KL, and Shlomchik MJ (2014). CD80 and PD-L2 define functionally distinct memory B cell subsets that are independent of antibody isotype. Nat. Immunol 15, 631–637. [PubMed: 24880458]

Highlights

- Hemozoin engages NLRP3 to reduce CD8α$^+$ dendritic cell (DC) number and function
- Impaired DC responses compromise the B cell helper functions of CD4$^+$ T cells
- The accumulation of hemozoin reduces memory B cell and plasma cell responses
- NLRP3 deficiency boosts humoral immune memory-mediated protection

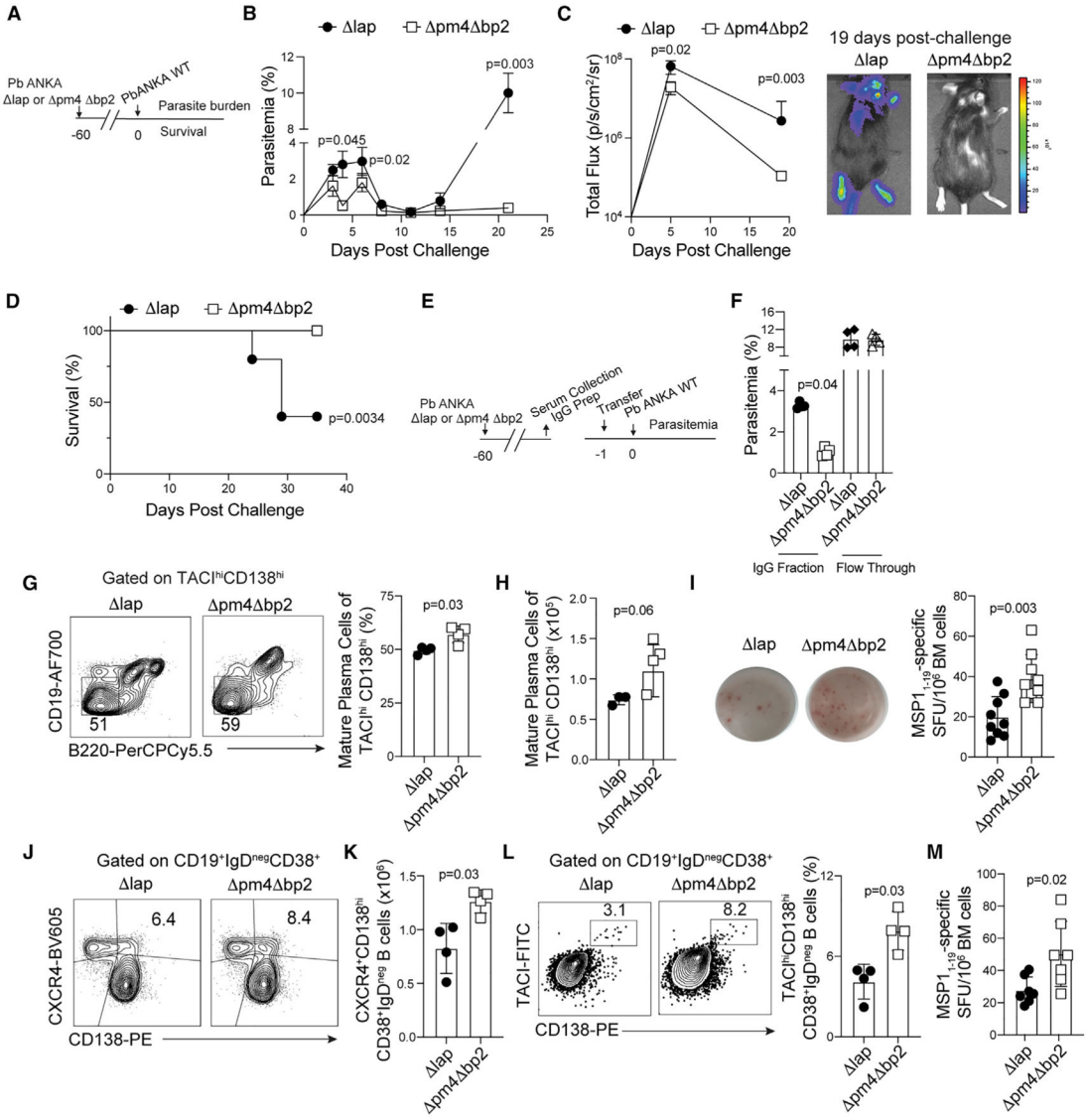

Figure 1. Hemozoin limits humoral immune memory responses

(A) C57BL/6 mice were infected with either Δ*pm4*Δ*bp2* or Δ*lap* parasites. After 60 days, immune mice were challenged with virulent WT *Pb*-ANKA-luc.

(B) The kinetics of peripheral parasite burden.

(C) Quantification (left) of parasite load as determined by whole-body bioluminescence following virulent *Pb*-ANKA-luc challenge. Images (right) on day 19 post-challenge.

(D) Survival of Δ*pm4*Δ*bp2 and* Δ*lap*-immune mice following virulent *Pb*-ANKA-luc challenge.

(E) IgG was purified from the indicated immune mice and either purified IgG or the unbound flow-through was transferred via tail vein to naive WT mice 1 day prior to challenge with virulent *Pb*-ANKA.

(F) Parasite burden at day 4 post-challenge.

(G and H) Representative flow plots, frequency (G), and (H) number of mature plasma cells ($B220^{neg}CD19^{neg}CD138^{hi}TACI^{hi}$) in the bone marrow at day 40 p.i.

(I) Number of $MSP1_{1–19}$-specific plasma cells in the bone marrow at day 40 p.i.
(J and K) Representative flow plots (J) and quantification of (K) splenic $IgD^{neg}CD38^{+}CD138^{hi}$ LLPC precursors expressing CXCR4 at day 14 p.i.
(L and M) Frequency of (L) bone-marrow $IgD^{neg}CD38^{+}CD138^{hi}TACI^{hi}$ plasma cells and (M) $MSP1_{1–19}$-specific IgG secreting cells recovered from the bone marrow of immune mice at day 28 p.i.
Data (mean ± SEM) in (B)–(D) and (mean ± SD) in (I) and (M) are the summary data from two independent experiments. Data (mean ± SD) in (F) and (J)–(L) are representative of two independent experiments with n = 4. Data (mean ± SD) in (G) and (H) are representative of three experiments with n = 4 (see also Figure S1).

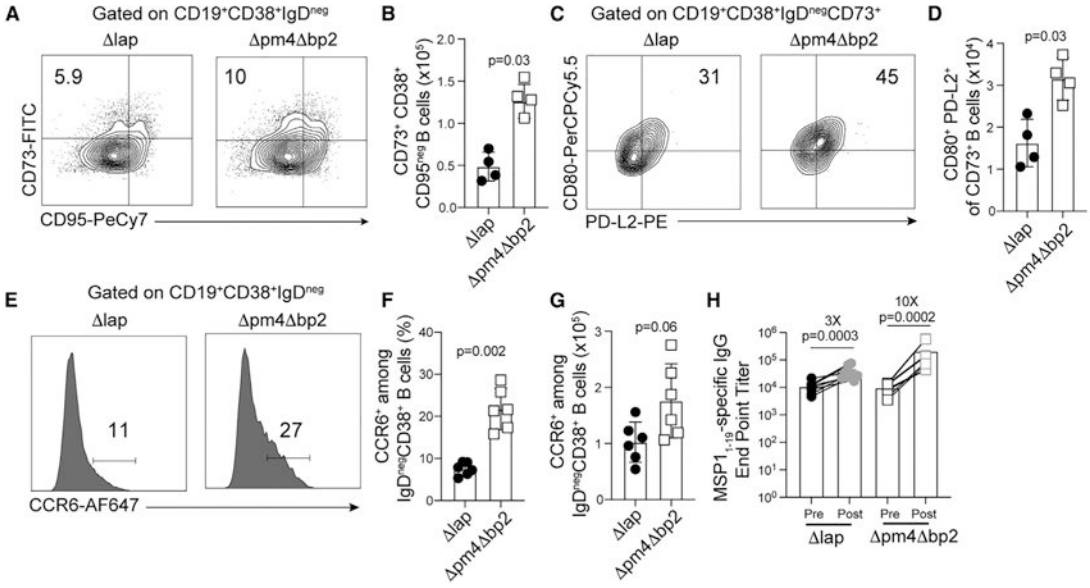

Figure 2. Hemozoin constrains the number and function of memory B cells

C57BL/6 mice were infected with Δ*pm4*Δ*bp2* and Δ*lap* parasites.

(A–D) Representative flow plots (A) and quantification (B) of splenic $CD19^{+}CD38^{+}IgD^{neg}CD73^{+}CD95^{neg}$ MBC and the frequency (C) and number (D) of splenic $CD19^{+}CD38^{+}IgD^{neg}CD73^{+}CD80^{+}PD\text{-}L2^{+}$ MBC by day 30 p.i.

(E) Representative histograms describing frequency (F) and number (G) of $CCR6^{+}CD19^{+}CD38^{+}IgD^{neg}$ MBC.

(H) Δ*pm4*Δ*bp2* and Δ*lap*-immune mice were challenged with virulent *Pb*-ANKA. Sera were collected before (pre) and 5 days after (post) challenge and $MSP1_{1–19}$-specific IgG endpoint titers were quantified. Data (mean ± SD) in (A)–(D) and are representative of three independent experiments with n = 4–5. Data (mean ± SD) in (E)–(H) are the summary data of two independent experiments.

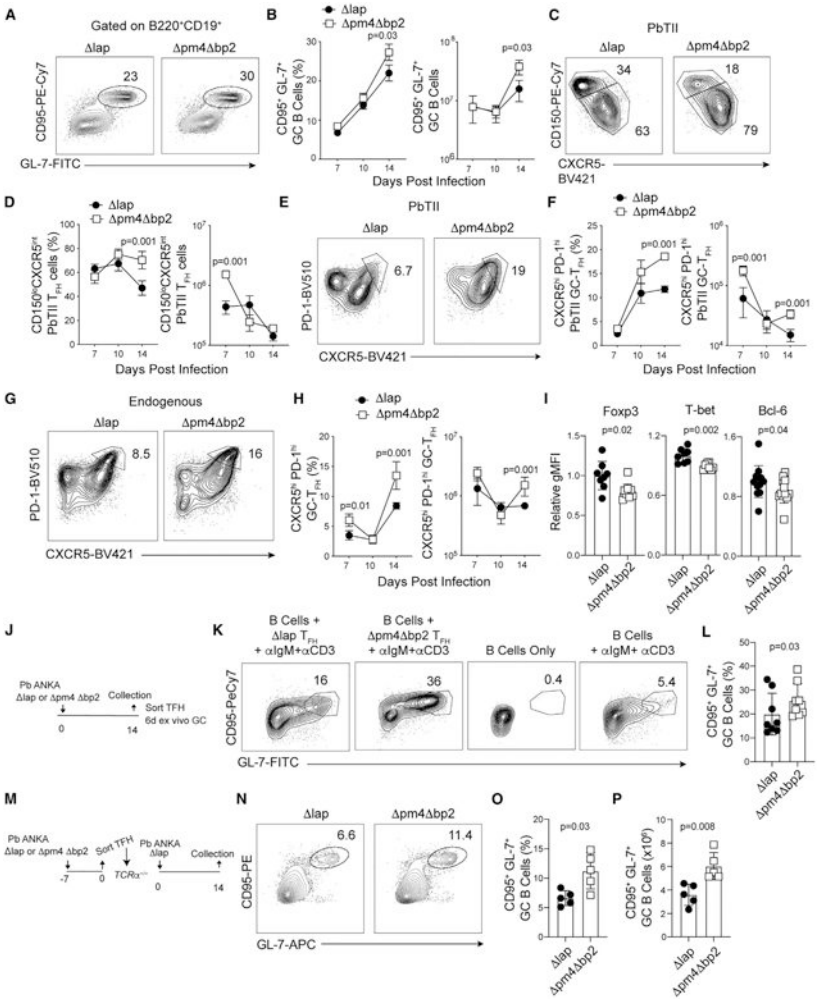

Figure 3. Hemozoin impairs the germinal center response

Parasite-specific CD4 T cells (PbTII) were transferred to C57BL/6 mice 1 day prior to infection with either Δ*pm4*Δ*bp2* or Δ*lap* parasites. Splenic T_{FH} and GC B cell responses were evaluated.

(A–F) Representative plots (A) and frequency and number (B) of GC B cells ($B220^+CD19^+CD95^+GL\text{-}7^+$) on d14 p.i. T_{FH} precursors ($CD150^{lo}CXCR5^{int}$) (C and D) and mature GC-T_{FH} ($CXCR5^{hi}PD\text{-}1^{hi}$) expansion (E and F) among donor-derived PbTII cells.

(G and H) Frequency (G) and summary quantification (H) of mature GC-T_{FH} ($PD\text{-}1^{hi}CXCR5^{hi}$) among polyclonal endogenous CD4 T cells.

(I) Relative expression (gMFI) of Foxp3, T-bet, and Bcl-6 in polyclonal GC-T_{FH} cells on day 14 p.i.

(J) Polyclonal GC-T_{FH} cells were sort purified from spleens day 14 p.i. and co-cultured for 6 days with purified naive B cells.

(K and L) Representative flow plots (K) and summary (L) of GC B cell ($B220^+CD19^+CD95^+GL\text{-}7^+$) frequency following co-culture.

(M) Polyclonal T_{FH} cells were sort purified from spleens of Δ*pm4*Δ*bp2* and Δ*lap*-infected mice day 7 p.i. and transferred to *Tcra*$^{-/-}$ mice. *Tcra*$^{-/-}$ mice were infected with Δ*lap* parasites and GC responses were assessed on 14 p.i.

(N–P) Representative flow plots (N) and summary of GC B cell ($B220^+CD19^+CD95^+GL\text{-}7^+$) frequency (O) and number (P).

Data (mean ± SEM) in (A)–(H) are representative of four experiments with n = 4–5. Data (mean ± SD) in (J)–(L) are the summary data from two independent experiments. Data (mean ± SD) in (M)–(P) are representative of two independent experiments with n = 5 (see also Figure S2).

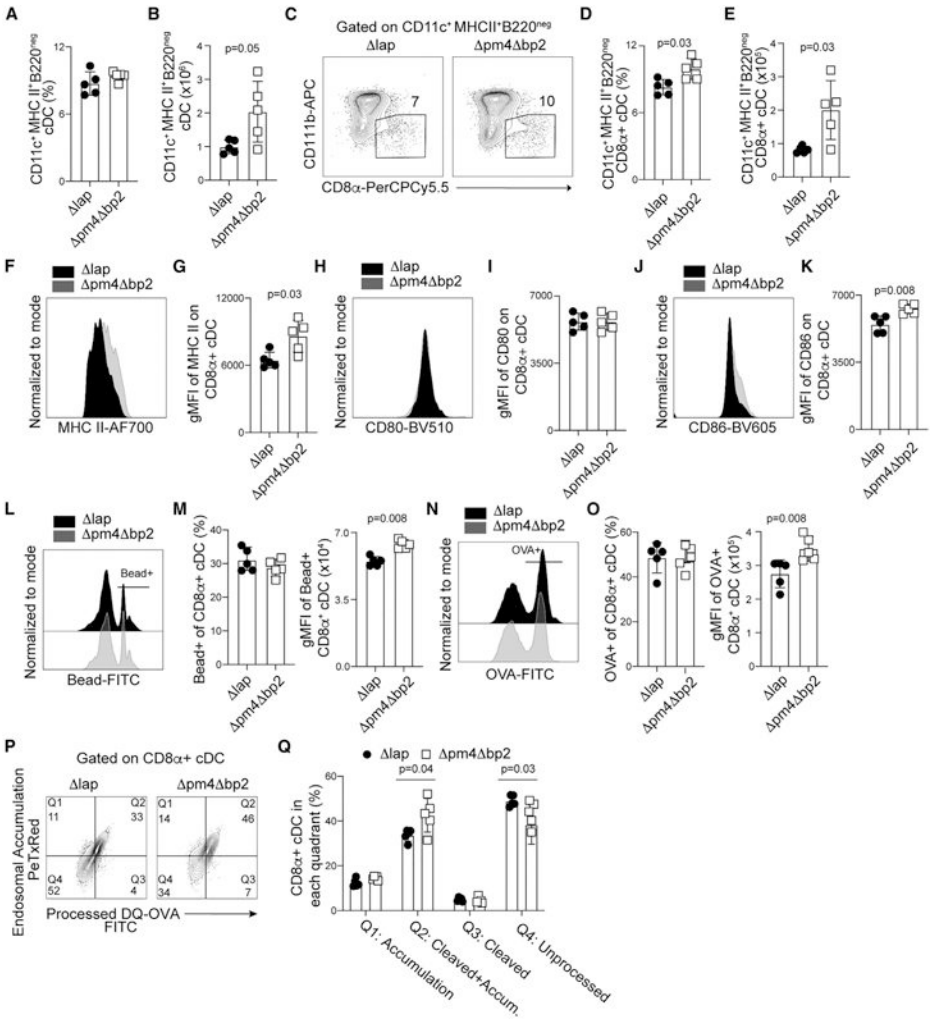

Figure 4. Hemozoin limits dendritic cell numbers and functions

C57BL/6 mice were infected with either Δ*pm4*Δ*bp2* or Δ*lap* parasites, spleens were harvested on day 4 p.i., and DCs were liberated by digestion as described in STAR Methods.

(A–E) Frequency and number of $CD11c^{+}MHCII^{+}B220^{neg}$ conventional DCs (A and B) and $CD11b^{neg}CD8\alpha^{+}$ cDC1 (C–E).

(F and G) Representative flow plots (F) and summary of MHC II expression (gMFI) (G) on $CD11b^{neg}CD8\alpha^{+}$ cDC1.

(H–L) Representative flow plots and summary data of CD80 (H and I) and CD86 (J and K) expression on $CD11b^{neg}CD8\alpha^{+}$ cDCs.

(L and M) Representative flow plots (L) and quantification of $bead^{+}CD11b^{neg}CD8\alpha^{+}$ cDCs (left) and fluorescence intensity of phagocytosed microbeads (gMFI) (right) (M).

(N and O) Representative flow plots of OVA-488 uptake (N), frequency of $OVA^{+}CD8\alpha^{+}$ cDC (O, left), and fluorescence intensity of phagocytosed OVA (gMFI) (O, right).

(P and Q) Flow plots and summary data of DQ-OVA protein processing assay. Data (mean ± SD) in all experiments are representative of two independent experiments with n = 5 (see also Figure S3).

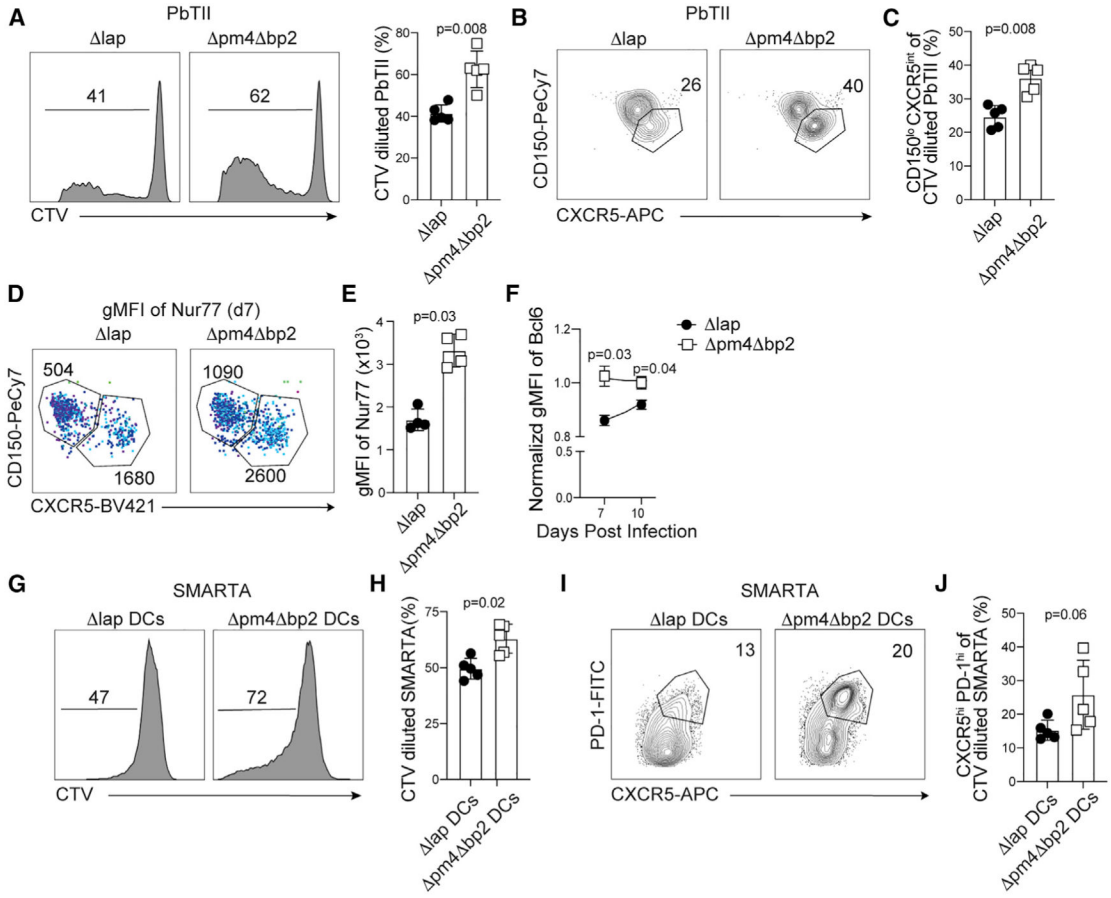

Figure 5. Optimal T_{FH} expansion is impaired by hemozoin

CTV-labeled PbTII cells were transferred into mice 1 day prior to infection with either Δ*pm4*Δ*bp2* or Δ*lap*-infected parasites and harvested 4 days later.

(A) Representative histograms and quantification of CTV dilution among PbTII cells.

(B and C) Flow plots (B) and summary (C) of CD150 and CXCR5 expression by CTV diluted PbTII.

(D) gMFI of Nur77 in $CD150^{lo}CXCR5^{int}T_{FH}$ and $CD150^{hi}CXCR5^{lo}T_H1$ PbTII $CD4^+$ T cells on day 7 p.i. with light blue corresponding to increased gMFI. Numbers on flow plots are gMFI.

(E) Summary of Nur77 gMFI among $CD150^{lo}CXCR5^{int}T_{FH}$

(F) Normalized Bcl-6 expression by PbTII T_{FH} collected on days 7 and 10 p.i. with Δ*pm4*Δ*bp2* or Δ*lap*. CTV-labeled SMARTA cells were cocultured for 4 days with GP-66 pulsed cDCs isolated from either Δ*pm4*Δ*bp2* or Δ*lap*-infected mice.

(G and H) Histogram of CTV dilution (G) and summary (H) data collected from SMARTA cells on d4 of *in vitro* culture.

(I and J) Flow plots (I) and summary (J) of PD-1 and CXCR5 expression by CTV diluted SMARTA cells.

Data (mean ± SD) are representative of two independent experiments with n = 4–5 (see also Figure S4).

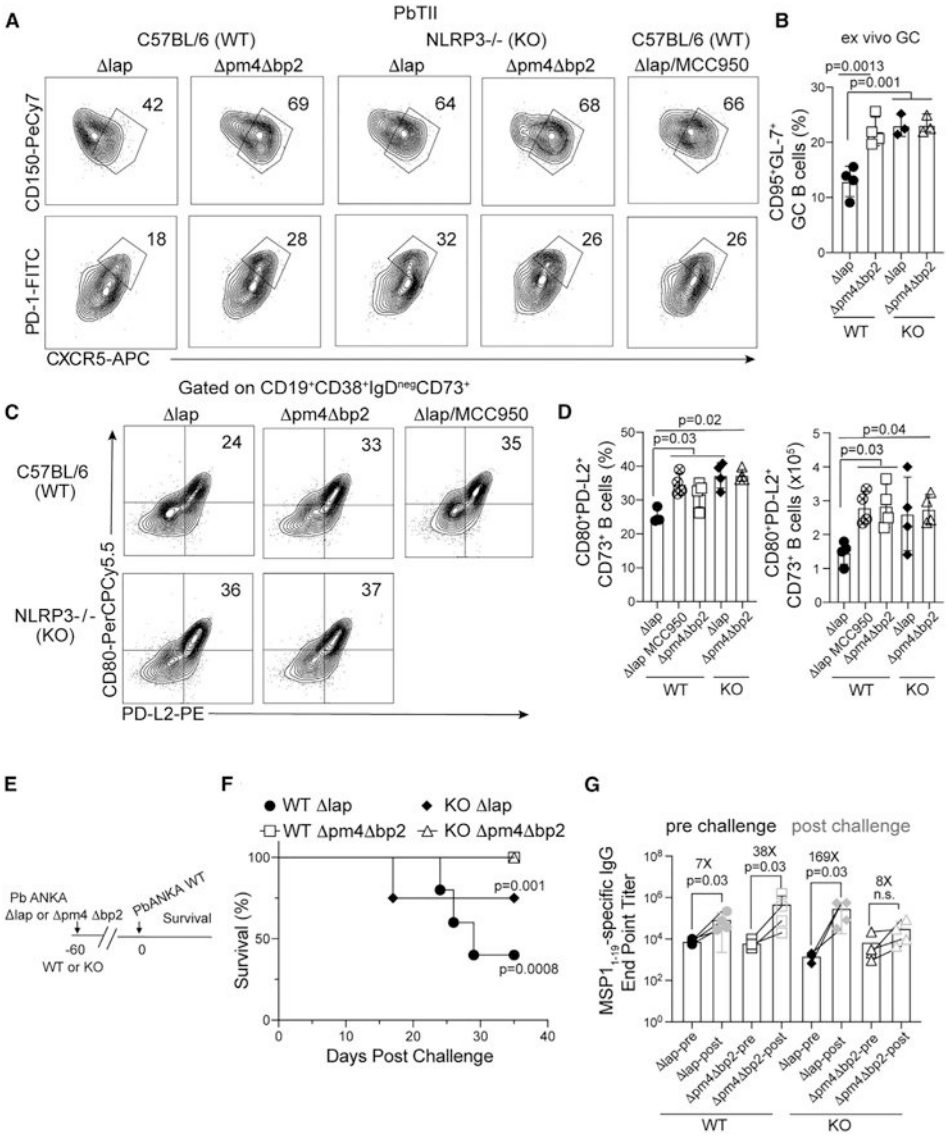

Figure 6. Hemozoin-mediated impairments in humoral immunity are governed by NLRP3

PbTII cells were transferred to C57BL/6 and NLRP3$^{-/-}$ mice 1 day prior to infection with either Δ*pm4*Δ*bp2* or Δ*lap* parasites. Splenic GC responses were evaluated on day 14 p.i.

(A) Representative flow plots of CD150^{lo}CXCR5^{int} T_{FH} and CXCR5^{hi}PD-1^{hi} GC-T_{FH} populations.

(B) CXCR5^{hi}PD-1^{hi} GC-T_{FH} cells were sort purified on day 14 p.i., co-cultured with naive B cells, and the frequency of CD95^{+}GL-7$_{+}$ GC B cells was quantified after 5 days.

(C and D) Representative flow plots (C) and frequency (D) of CD80^{+}PD-L2^{+}CD73^{+}CD38^{+}CD95^{neg} MBC on day 28 p.i.

(E) C57BL/6 and NLRP3$^{-/-}$ mice were immunized with Δ*pm4*Δ*bp2* and Δ*lap* parasites 60 days prior to challenge with a virulent *Pb*-ANKA strain.

(F) Frequency of immune mice that survived virulent *Pb*-ANKA challenge.

(G) MSP1$_{1–19}$-specific IgG endpoint titers 1 day prior to (pre) and 5 days after (post) virulent *Pb*-ANKA challenge.

Data (mean ± SD) in (A)–(D) are representative of three experiments with n = 3–4. Data (mean ± SD) in (E)–(G) are representative of two independent experiments with n = 3–4 per experimental group (see also Figure S5).

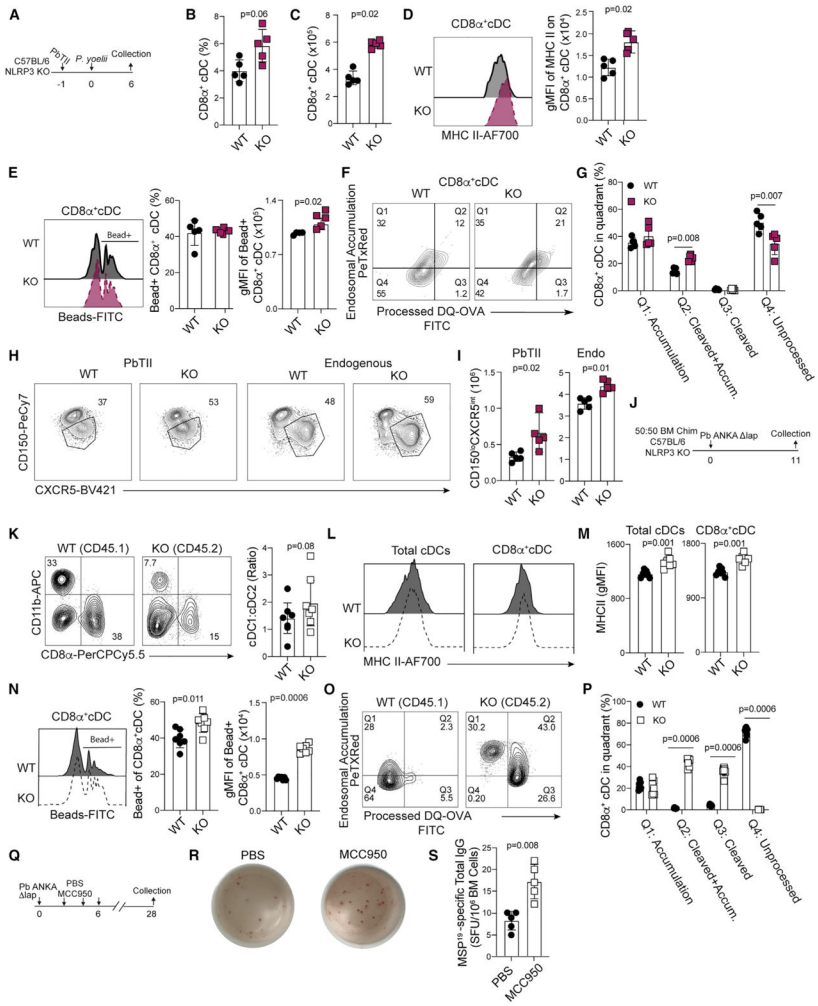

Figure 7. Hemozoin impairs dendritic functions via cell-intrinsic NLRP3 activity

(A) Experimental design for samples depicted in (B)–(I) from C57BL/6 (WT) and NLRP3$^{-/-}$ (KO) mice infected with *P. yoelii 17*XNL parasites.

(B and C) Summary CD11b^{neg}CD8α^{+} cDC1 frequency (B) and number (C) in WT and NLRP3 KO mice.

(D) Histogram and summary of MHC II expression in CD8α^{+} cDC1.

(E) Histograms of bead uptake, summary graph of the frequency of bead positive CD8α^{+} cDC1 (center), and gMFI of phagocytosed beads (right).

(F and G) Flow plots (F) and summary (G) of DQ-OVA antigen processing assay. The frequency of CD11b^{neg}CD8α^{+} cDC1 in each quadrant is depicted.

(H and I) Flow plots (H) and number (I) of CD150^{lo}CXCR5^{int} T_{FH} among parasite-specific (left) and polyclonal (right) CD4 T cells on day 6 p.i.

(J) Experimental schematic for C57BL/6:NLRP3$^{-/-}$ (50:50) bone-marrow chimera generation.

(K) Ratio of CD11b^{+}CD8α^{neg} cDC2 and CD11b^{neg}CD8α^{+} cDC1 recovered from chimeras on d11 p.i.

(L and M) Histograms and quantification of MHC II expression by total cDC and $CD11b^{neg}CD8\alpha^{+}$ cDC1.
(N) Flow plots of bead uptake (left), summarized frequency of fluorescent $bead^{+}$ $CD11b^{neg}CD8\alpha^{+}$ cDC1 (center), and gMFI of fluorescent beads are quantified (right).
(O) DQ-OVA antigen-processing assay.
(P) The frequency of $CD11b^{neg}CD8\alpha^{+}$ cDC1 in each quadrant is quantified.
(Q) C57BL/6 (WT) mice were administered either MCC950 or PBS i.p. during the first 6 days of infection, and bone marrow was collected on day 28 for quantification of MSP_{19} LLPC via ELISPOT.
(R and S) Representative ELISPOT photos (R) and summary data (S).
Data (mean ± SD) in (A)–(I) and (Q)–(S) are representative of two independent experiments with n = 5. Data (mean ± SD) in (K)–(P) are the summary data collected from two independent experiments (see also Figure S6).

KEY RESOURCES TABLE

Reagent or resource	Source	Identifier
Antibodies		
Purified anti-mouse CD3	Biolegend	Cat#100202; RRID: AB_312659
Anti-mouse CD16/32 (Fc-Block)	BioXCell	Cat#BE0307, RRID: AB_2736987
Biotin SP-conjugated Affinipure Goat-anti-IgG (H+L) F(ab)	Jackson Immunoresearch	Cat#112-065-167, RRID: AB_2338179
Purified rat anti-mouse CXCR5	BD Biosciences	Cat#551961, RRID: AB_394302
Anti-mouse CXCR4-BV605 (clone: L276F12)	Biolegend	Cat#146519, RRID: AB_2687359
Anti-mouse CD150-PeCy7 (clone:TC15-12G12.2)	Biolegend	Cat#115914, RRID: AB_439797
Anti-mouse CD267-PE (clone 8F10)	Biolegend	Cat#133403, RRID: AB_2203542
Anti-mouse IgD-PeDazzle 594 (clone: 11-26c.2a)	Biolegend	Cat#405742, RRID: AB_2571985
Anti-mouse CD86-BV605 (clone:GL1)	Biolegend	Cat#105037, RRID: AB_11204429
Anti-mouse CD80-BV510 (clone:16-10A1)	Biolegend	Cat#104741, RRID: AB_2810337
Anti-mouse CD80-PerCPCy5.5 (clone:16-10A1)	Biolegend	Cat#104722, RRID: AB_2291392
Anti-mouse CD11c-PE Cy7 (clone:N418)	Biolegend	Cat#117318, RRID: AB_493568
Anti-mouse CD38-Pac Blue (clone:90)	Biolegend	Cat#102720, RRID: AB_10613468
Anti-mouse CD95-FITC (clone: Jo2)	BD Biosciences	Cat#554257, RRID: AB_395329
Anti-mouse MHCII-AF700 (clone:M5/114.15.2)	Biolegend	Cat#107622, RRID: AB_493727
Anti-mouse CCR6-AF647 (clone:29-2L17)	Biolegend	Cat#129808, RRID: AB_1227497
Anti-mouse CD138 Pac Blue (clone 281-2)	Biolegend	Cat#142523, RRID: AB_2565621
Anti-mouse B220-PerCP-Cy5.5 (clone:RA3-6B2)	Biolegend	Cat#103236, RRID: AB_893354
Anti-mouse B220-PE (clone:RA3-6B2)	Invitrogen	Cat#12-0452-83, RRID: AB_465672
Anti-mouse CD11b-APC (clone: M17/70)	Biolegend	Cat#101212, RRID: AB_312795
Anti-mouse CD4-PerCP-Cy5.5 (clone:GK1.5)	Biolegend	Cat#100434, RRID: AB_893324
Anti-mouse CD8-PerCP-Cy5.5 (clone: 53-6.7)	Biolegend	Cat#100734, RRID: AB_2075238
Anti-mouse CD19-AF700 (clone: 6D5)	Biolegend	Cat#115528, RRID: AB_493735
Anti-mouse CD45.2-PE (clone: 104)	Biolegend	Cat#109808, RRID: AB_313445
Anti-mouse CD273-PE (clone: TY25)	Biolegend	Cat#107206, RRID: AB_2162011
Anti-mouse F4/80-PE (clone: BMB)	Biolegend	Cat#123110, RRID: AB_893486
Anti-mouse Foxp3-PeCy7 (clone: 3G3)	Tonbo	Cat#60-5773-U100, RRID: AB_2621869
Anti-mouse Bcl-6-AF647 (clone IG191E/A8)	Biolegend	Cat#648305, RRID: AB_2565298
Anti-mouse Tbet-BV605 (clone: 4B10)	Biolegend	Cat#644817, RRID: AB_11219388
Anti-mouse CD95-PeCy7 (clone: Jo2)	BD PharMingen	Cat#557653, RRID: AB_396768
Anti-mouse CD73-FITC (clone: TY/11.8)	Biolegend	Cat#127220, RRID: AB_2716076
Anti-mouse PD-1-BV510 (clone: RPM1-30)	Biolegend	Cat#135241, RRID: AB_2715761
Anti-mouse PD-1-FITC (clone: RPM1-30)	Thermo Fisher Scientific	Cat#11998181, RRID: AB_465466
Anti-mouse CD45.1-PacBlue (clone: A20)	Biolegend	Cat#110722, RRID: AB_492866
Anti-mouse CD90.1-PeDazzle (clone: OX-7)	Biolegend	Cat#202524, RRID: AB_1595635
Anti-mouse CD44-AF700 (clone:IM7)	Biolegend	Cat#103026, RRID: AB_493713
Anti-mouse CD44-FITC (clone:IM7)	Biolegend	Cat#103006, RRID: AB_312957
Anti-mouse CD11a-FITC (clone:M17/4)	Biolegend	Cat#101106, RRID: AB_312779

Reagent or resource	Source	Identifier
Anti-mouse GL7-FITC (Clone:GL7)	Biolegend	Cat#144603, RRID: AB_2561696
Chemicals, peptides, and recombinant proteins		
Hemozoin	InvivoGen	Cat#tlrl-hz
MCC950 (NLRP3 Inhibitor)	Sigma	Cat#256373-96-3
D-luciferin	Promega	Cat#P1043
Collagenase IV	GIBCO	Cat#17104019
DNase I	Roche	Cat#10104159001
Cell Trace Violet	Invitrogen	Cat#C34557
streptavidin-BV421	BD Biosciences	Cat#563259
streptavidin-APC	BD Biosciences	Cat#405207
Fluoresbrite carboxylate microsphere YG 0.5 μm	Polysciences	Cat#15700
OVA-488	Molecular Probes	Cat#O34781
DQ-OVA	Molecular Probes	Cat#D12053
B Cell Isolation Kit	Miltenyi Biotec	Cat#130-090-862
GP_{66-77} peptide	BioSynthesis Inc.	Cat#Custom
Recombinant $MSP1_{19}$ ($yPyMSP1_{19}XL$)	BEI Resources	Cat#MRA-48
Critical commercial assays		
SureBlue TMB Peroxidase	Sera Care	Cat#5120-0077
TMB Stop Solution	Sera Care	Cat#5150-0021
LEGENDplex immunoassay	Biolegend	Cat#740150
Experimental models: Organisms/strains		
C57BL/6J	Jackson Laboratories	Cat#RRID:IMSR_JAX:000664
C57BL/6-Tg(Nr4a1-EGFP/cre)820Khog/J	Jackson Laboratories	Cat#RRID:IMSR_JAX:016617
B6.129S6-$Nlrp3^{tm1Bhk}$/J	Jackson Laboratories	Cat#RRID:IMSR_JAX:021302
B6.SJL-$Ptprc^{a}$ $Pepc^{b}$/BoyJ	Jackson Laboratories	Cat#RRID:IMSR_JAX:002014
B6.Cg-$Ptprc^{a}$ $Pepc^{b}$ Tg(TcrLCMV)1Aox/PpmJ	Jackson Laboratories	Cat#RRID:IMSR_JAX:030450
P. berghei ANKA	BEI-MR4	Cat#MRA-871
P. berghei ANKA line 676m1cl1	BEI-MR4	Cat#MRA-868
P. yoelii (clone 17XNL)	BEI-MR4	Cat#MRA-593
P. berghei ANKA Δpm4Δbp2 and Δlap	A gift from Dr. Chris Janse (Leiden University)	https://rupress.org/jem/article/212/6/893/41818/Replication-of-Plasmodium-in-reticulocytes-can
Software and algorithms		
Flowjo v10.5.0	Treestar	https://www.flowjo.com/solutions/flowjo/downloads
Prism v9	Graphpad	https://www.graphpad.com
Excel v16.16.20 9	Microsoft	https://www.microsoft.com/en-us/microsoft-365/excel
Living Image	Perkin Elmer	https://www.perkinelmer.com/product/spectrum-200-living-image-v4series-1-128113
Other		
Biotek plate reader	Biotek	N/A
BD LSR II	BD	N/A
BD FACSVerse	BD	N/A

Reagent or resource	Source	Identifier
IVIS Lumina S5	Perkin Elmer	N/A